AD-A181 131

RADC-TR-86-225
Final Technical Report
February 1987

PLANAR MULTIMODE FIBER OPTIC COUPLERS

TRW Electro-Optics Research Center

Charles Asawa and Talal Findakly

APPROVED FOR PUBLIC RELEASE; DISTRIBUTION UNLIMITED

ROME AIR DEVELOPMENT CENTER
Air Force Systems Command
Griffiss Air Force Base, NY 13441-5700

This report has been reviewed by the RADC Public Affairs Office (PA) and is releasable to the National Technical Information Service (NTIS). At NITS it will be releasable to the general public, including foreign nations.

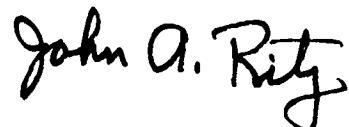RADC-TR-86-225 has been reviewed and is approved for publication.

APPROVED: *Richard Payne*
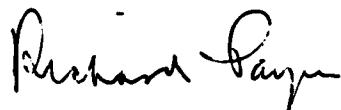
RICHARD PAYNE
Project Engineer

APPROVED: *Harold Roth*

HAROLD ROTH
Director of Solid State Sciences

FOR THE COMMANDER: *John A. Ritz*

JOHN A. RITZ
Directorate of Plans & Programs

A181 131

REPORT DOCUMENTATION PAGE

1a. REPORT SECURITY CLASSIFICATION UNCLASSIFIED		1b. RESTRICTIVE MARKINGS N/A		
2a. SECURITY CLASSIFICATION AUTHORITY N/A		3. DISTRIBUTION / AVAILABILITY OF REPORT Approved for public release; distribution unlimited		
2b. DECLASSIFICATION / DOWNGRADING SCHEDULE N/A				
4. PERFORMING ORGANIZATION REPORT NUMBER(S) N/A		5. MONITORING ORGANIZATION REPORT NUMBER(S) RADC-TR-86-225		
6a. NAME OF PERFORMING ORGANIZATION TRW Electro Optics Research Center	6b. OFFICE SYMBOL (If applicable)	7a. NAME OF MONITORING ORGANIZATION Rome Air Development Center (ESOC)		
6c. ADDRESS (City, State, and ZIP Code) One Space Park Building 135, Room 1744 Redondo Beach CA 90278		7b. ADDRESS (City, State, and ZIP Code) Hanscom AFB MA 01731-5000		
8a. NAME OF FUNDING / SPONSORING ORGANIZATION Rome Air Development Center	8b. OFFICE SYMBOL (If applicable) ESOC	9. PROCUREMENT INSTRUMENT IDENTIFICATION NUMBER F19628-84-C-0123		
8c. ADDRESS (City, State, and ZIP Code) Hanscom AFB MA 01731-5000		10. SOURCE OF FUNDING NUMBERS		

PROGRAM ELEMENT NO. 61102F	PROJECT NO. 2306	TASK NO. J2	WORK UNIT ACCESSION NO. 50

11. TITLE (Include Security Classification)
PLANAR MULTIMODE FIBER OPTIC COUPLERS

12. PERSONAL AUTHOR(S)
Charles Asawa, Talal Findakly

13a. TYPE OF REPORT Final	13b. TIME COVERED FROM Jul 84 TO Apr 86	14. DATE OF REPORT (Year, Month, Day) February 1987	15. PAGE COUNT 72

16. SUPPLEMENTARY NOTATION
N/A

17.	COSATI CODES		18. SUBJECT TERMS (Continue on reverse if necessary and identify by block number)
FIELD	GROUP	SUB-GROUP	Multimode optical coupler
17	02		ion-exchanged waveguide
20	06		thallium-sodium ion exchange

19. ABSTRACT (Continue on reverse if necessary and identify by block number)
This report presents the results of our 1.75 years investigation of the fabrication of multimode star and access couplers in glass using the thallium-sodium ion exchange method. Four-port access and eight port transmission star couplers were fabricated on BK-7 glass. Electric-field-assisted thermal ion exchange was used to form the couplers. Numerous waveguide coupler designs were used to fabricate the couplers. The photolithographic masks were designed with varying waveguide widths and mixing lengths. The best mask material was found to be silicon dioxide of 5000 angstroms thickness. Measurements were performed on efficiencies and distribution uniformities on both the single diffusion and second diffusion samples. Excellent first diffusion couplers were fabricated. Less than 0.2 dB and 1.0 dB non-uniformity in the splitting ratios were measured for the best first diffusion 2x2 and 4x4 couplers, respectively. Experiments were performed to bury the couplers below the surface of the glass with a second electric-field assisted diffusion for the purpose of reducing optical loss at the surface. Partially buried waveguides were formed but these waveguides exhibited (over)

20. DISTRIBUTION / AVAILABILITY OF ABSTRACT ☒ UNCLASSIFIED/UNLIMITED ☐ SAME AS RPT ☐ DTIC USERS	21. ABSTRACT SECURITY CLASSIFICATION UNCLASSIFIED	
22a. NAME OF RESPONSIBLE INDIVIDUAL Richard Payne	22b. TELEPHONE (Include Area Code) (617) 377-2234	22c. OFFICE SYMBOL RADC (ESOC)

DD FORM 1473, 84 MAR 83 APR edition may be used until exhausted
All other editions are obsolete

Block 19. Abstract (Cont'd)

greater scattering than the first diffusion waveguides.

Accesion For		
NTIS CRA&I	☑	
DTIC TAB	☐	
Unannou..ced	☐	
Justif·catio::		
By		
Di..t ib tio ./		
Availability Codes		
Dist	Aval .. :t / or Sp..cial	
A-1		

Table of Contents

List of Figures

List of Tables

1. INTRODUCTION AND SUMMARY

1.1 Introduction

This is the final report on Contract No. F19628-84-C-0123 entitled "Planar Multimode Fiber Optic Couplers", covering the work performed between July 16, 1984 through April 15, 1986.

As short distance multimode fiber optic communication networks proliferate, the need for multimode fiber optic access and star couplers will increase. These couplers must exhibit good output power splitting uniformity, low loss, environmental ruggedness, compatibility with commercial multimode fibers, reproducibility and low production cost. Thus far the most successful multimode coupler developed is the biconically tapered fused fiber coupler. However, the fused fiber coupler may not adequately meet some of the above-mentioned requirements, particularly those imposed by the harsh military environment.

The object of the present program was to develop the technology of electric-field-assisted $T\ell^+$-Na^+ ion-exchange waveguides in glass substrates and to design and fabricate a 4-port access and 8-port transmission star couplers using the developed technology. Couplers fabricated monolithically on glass substrates could have many advantages over the fused fiber couplers. The monolithic couplers could form a rugged, environmentally stable package. Furthermore, the coupler pattern can be defined on the glass substrate with standard photolithographic techniques, which can lead to low cost in volume production.

The summary section of this report gives a brief outline of the accomplishments under this program.

1

1.2 Summary

During this program, methods of fabricating multimode waveguides in glass by the electric field assisted Tl^+-Na^+ ionic exchange were developed and used to fabricate 4-port access and 8-port transmission multimode star couplers. The output power distribution uniformity for the 2x2 and 4x4 couplers was < 0.5 dB and < 1 dB, respectively, and the waveguide propagation loss was ~ 0.1 dB/cm. The numerical aperture depended upon the Tl^+ concentration for the first diffusion and varied from 0.19 to 0.23. The second diffusion generally lowered the NA to ~0.11 to 0.15.

During the first phase of the program, the apparatus to carry out the highly toxic Tl^+ ion-exchange experiments was designed, constructed, and tested for safe operation. Materials such as sulfates of Na, K, Zn, Tl, etc. were ordered along with optical quality Bk-7 glasses. A mask was designed to allow the study of waveguide size and structure geometry as a function of diffusion conditions. Procedures for the electric field assisted diffusion were developed and incorporated with the apparatus design.

Iterations during the early stages of the program were necessary to determine the optimum diffusion parameters such as temperature, time, electric field, salt concentration, and masking material. Based on this information, thallium enriched star and access couplers were fabricated, polished and evaluated for transmission, output power coupling uniformity, size, shape, and numerical aperture. Despite the problems encountered such as glassware breakage, delays in replacements, logistical problems in handling toxic materials, delays due to health and safety inspection and consequent modifications, the program goals were met.

The first diffusion thallium couplers exhibited exceptionally low scattering and good distribution of optical power. However, the second electric field assisted diffusion to bury the thallium waveguides resulted in couplers with increased amounts of scattering. The scattering is believed to be due to scattering sites resulting from differing electric field drift velocities for the thallium, sodium and potassium impurities.

2

The potassium impurity was included to stabilize the molten mixture during the initial study of melting points.

Lack of thallium sulfate availability from normal commercial sources during the latter part of this program required th. repeated use of the old thallium mixture. The resulting waveguides had lower NA's (~.11) than desirable and some excess scattering.

During the last week of this program a new supply of thallium sulfate was finally received. An electric-field-assisted diffusion waveguide coupler prepared with a new mixture, without potassium sulfate, yielded one of the best single diffusion couplers fabricated to date, with low scattering, excellent coupling distribution and NA ~ 0.20.

2. TECHNICAL DISCUSSION

2.1 The Ion-Exchange Technique: Background

Alkali ion exchange for the purpose of strengthening glass has been extensively studied in the past. Because of the advances in optical fiber communications and the emergence of integrated optics in the last 15 years, the usefulness of this process for optical waveguide formation in glass became the subject of numerous studies. For glass strengthening purposes, a large ion from an alkali salt melt is exchanged with a smaller ion in the glass to produce a compressive stress on the glass surface. While glass strength is not an important factor in light-guiding structures, the exchange process itself can be utilized to produce light-guiding structures since any alteration of the electronic structure of glass yields a refractive index change. The refractive index can be increased or decreased as a result of a combination of two major effects. The first effect relates to the atomic size of the exchanging ions. If a small ion such as Li^+ replaces a larger ion such as Na^+ or K^+, the glass network will collapse around the smaller ion to produce a more densely packed structure that usually has a higher refractive index. Conversely, if a larger ion replaces a smaller ion, the network expands to a less packed structure, yielding a lower refractive index. A second effect relates to the electronic polarizability of the exchanging ions. If an ion of larger electronic polarizability such as Tl^+ Cs^+, Ag^+, Rb^+, or K^+ replaces an ion of smaller polarizability such as Na^+, an increase in the refractive index will result, and vice versa. The increase in the refractive index can be shown to be related to the electronic polarizability in the following form[1]:

$$\Delta n = \frac{(n^2+2)^2}{6n} \frac{4\pi}{3V} \sum_i \Delta Q_i \alpha_i, \tag{1}$$

where n is the refractive index, V is volume, ΔQ_i is the number of ions type (i) replaced, and α_i is the electronic polarizability.

Sodium ions, present in common glasses such as soda limes and borosilicates, are known for their high mobility and therefore exchange

4

well with monovalent alkali ions. The extent and rate of exchange depend
on the activation energy, glass composition, temperature, molar fractions,
and various other parameters that govern the diffusion kinetics. The
diffusion kinetics of ion exchange for a binary exchange are described by
the following relationship

$$D_m = \frac{D_1 D_2 (N_1 + N_2)}{D_1 N_1 + D_2 N_2},$$

(2)

where D_m is the interdiffusion coefficient, D is the self-diffusion
coefficient, N is the ion concentration, and subscripts 1 and 2 refer to
the exchanging species. The inter-and self-diffusion coefficient have
strong composition dependence. The rate of ion exchange is controlled by
the slower mobile ions, and the mobility is reduced considerably by the
mixed-alkali effect. For light-guiding structures, however, it is
important first to consider the more directly relevant parameters as they
affect the change in refractive index. Table 1 lists the electronic
polarizability[2], ionic radius, melting and decomposition points of the
salts for monovalent ions that alter the refractive index of glass when
exchanged with Na^+ ions, and the index increase. This table provides the
possible options available in meeting certain waveguide requirements.

2.1.1 Alkali Ions for the Ion Exchange

As shown in Table 1, the monovalent alkali ions that yield an increase
in the refractive index of glass when exchanged with Na^+ ions include Li^+,
Cs^+, Rb^+, K^+, Ag^+, and Tl^+. During the past 15 years, considerable work
has been reported on the use of these ions for the formation of single-mode
and multimode waveguides in glass. The general characteristics of the ion-
exchange process associated with each of these ions is reviewed next.

2.1.1.1 Li^+ - Na^+ Ion Exchange

As mentioned earlier, the substitution of Li^+ ions for Na^+ ions
results in an increase in the refractive index, not because of lithium's
electronic polarizability, but because of its smaller ionic size compared
to Na^+, which yields a more densely packed structure. The index increase
is generally small

5

Table 1. Relevant Ion-Exchange Parameters

Ion	Electronic polarizability (λ=D) Å³	Ionic radius Å	Salts or Mixture Salts	Melting point °C (mol fraction)	Decomposition point °C	Index Increase
Na$^+$	0.41	0.95	NaNO$_3$	307	380	-
Li$^+$	0.03	0.65	LiNO$_3$	264	600	0.01
			LiSO$_4$ (0.8), K$_2$SO$_4$ (0.2)	524		0.015
Tℓ$^+$	5.2	1.49	TℓNO$_3$	206	430	0.1
			TℓSO$_4$	632	0.1	
Cs$^+$	3.34	1.65	CsNO$_3$	414		0.03
Ag$^+$	2.4	1.26	AgNO$_3$	212	444	0.09
Rb$^+$	1.98	1.49	RbNO$_3$	310		0.015
K$^+$	1.33	1.33	KNO$_3$	334	400	0.009
Ag$^+$	2.4	1.26	silver film			0.001
Ag$^+$	2.4	1.26	silver film field-assisted			0.025

* References in text.

6

(<0.015), making it suitable for single-mode waveguides but marginally acceptable for multimode waveguides of large numerical aperture. The diffusion of Li^+ ions in glass is fast due to their small size, which makes lithium attractive for producing thick multimode layers in reasonably short times. The losses of such layers are subject to question, however, since it is known that the collapse of the glass network around the small Li^+ ions near the surface at temperatures below the glass transition temperature results in surface deformations and microcracks for long diffusion times[3]. Light-focusing rods in lithium aluminosilicate glasses and planar guided layers in sodium aluminosilicate glasses were produced by Na^+ ~Li^+ ion-exchange from $NaNO_3$ and $LiNO_3$ sources, respectively, with an index change peak as high as 0.0018[4,5]. Attempts to bury the guided layers by double diffusion caused surface damage, but no figures on the losses were reported. A eutectic melt of Li_2SO_4 and K_2SO_4 was also used as a source for exchanging Li^+ ions with Na^+ ions in soda lime glass slides at high temperatures (575°C), yielding thick guiding layers in short diffusion times.[6,7] The waveguides so produced were 40 to 140 μm thick with Δn = 0.015 at the surface and had propagation losses of 1.2 dB/cm.

2.1.1.2 Cs^+, Rb^+ ~ Na^+ Ion Exchange

Cs^+ and Rb^+ ions can also provide an increase in the refractive index when exchanged with Na^+ ions due to the gain in electronic polarizability, as indicated in Table 1. Planar waveguides produced by Cs^+ ~ Na^+ ion exchange were reported in soda lime glass from a $CsNO_3$ source at 520°C. Due to its large size, Cs^+ diffuses slowly in glasses. Waveguides 8 μm deep were fabricated in 37 hr at 520°C.[8] The waveguides so formed had an index increase of 0.03 and an estimated loss of 1 dB/cm. The formation of similar waveguides by Rb^+ ~ Na^+ ion exchange was also reported.[8] The index increase in this case was smaller than that of Cs^+ (about 0.015), which is expected due to the lower electronic polarizability of Rb^+. No data were given on processing parameters and losses. Both Rb and Cs compounds present considerable toxic and fire hazards, which explains the limited work carried out using such materials.

2.1.1.3 $Ag^+ - Na^+$ Ion Exchange

The $Ag^+ - Na^+$ ion exchange is probably by far the most explored ion-exchange technique. However, considerable problems associated with the waveguide losses produced by this method remain unsolved. Ag^+ ions from $AgNO_3$ salt exchange very well with Na^+ ions in glass even at low temperatures, typically in the range 220 to 300°C. The strong interdiffusion between Na^+ and Ag^+ ions, coupled with a large index increase obtainable (typically 0.09 in soda lime glass,[9-13] and 0.22 in TiF6 glass[14]) result in highly multimode waveguides for diffusion periods of a few hours. The losses in such waveguides have been relatively high (often a few dB/cm). The refractive index can be adjusted below the saturation level by diluting the silver salts with sodium or potassium salts.[11,12] Lower silver concentration, and therefore Δn, usually results in lower losses. Recently, a new method of controlling the silver content, and therefore the refractive index, in silver ion-exchange waveguides was introduced using electrolytic release of silver ions from a silver rod electrode immersed in molten $NaNO_3$.[15] By controlling the current, the silver concentration in the salt, and therefore the rate of $Ag^+ - Na^+$ ion exchange, can be controlled, yielding the desired index change. The exchange was carried out at 330°C for 20 to 120 min on soda lime glass slides, yielding single and double mode waveguides with an index increase $\Delta n \simeq 0.005$. The losses varied with the glass type used. For example, Schott slides yielded 0.2 dB/cm, while Labmate slides yielded 1 dB/cm at 0.633 μm. The low Δn obtained implies very small silver concentration in the waveguides and explains the low loss reported in some of their samples.

Due to its compatibility with faster multimode waveguide formation, the electric-field-assisted silver ion-exchange technique has been used to fabricate deep planar layers as well as multimode star and access couplers. We have previously used this technique to fabricate 2x2 and 4x4 multimode couplers by employing a central mixing region connected to input and output ports through Y-junctions. Distribution uniformities of 0.5 dB and 1.0 dB were obtained for the 2x2 and 4x4 couplers, respectively. The losses were in the range of 1 to 1.5 dB/cm. The high losses commonly observed in silver ion-exchange waveguides are the result of silver ion reduction in glasses containing certain impurities. This issue is discussed next.

8

On a historic note, Ag^+ ion exchange dates back several hundred years, and possibly even more. In glass-manufacturing circles, Griesinger (Ulm, 1460) is often credited with having been the first to apply this technique (also known as staining) to window glasses. In fact, some stained church windows of the fifteenth century are some of the old examples of this technique for producing yellow colors and for shading other colored panes. Artists found this method very convenient since it enabled them to produce permanent colors without destroying the natural fire polish of the glass surface. The process of baking a vitreous surface coated with silver containing a mixture of clay or ochre in order to produce a variety of colors was known and practiced long before Griesinger. Old Persian pottery and Moorish pieces of glazed earthenware were decorated this way. In the ninth century, the African Moors were skilled in this art, and, by varying the composition of the pastes, time, and temperature of the baking process, they produced yellow to brown shades and metallic lusters. Through the Spanish Moors this art came to Spain, Italy, and France and thus spread over Europe.

The production of silver stain is based on the principle of silver ion exchange with the existing alkali ions in the glass at temperatures below the softening range. After the silver ions penetrate through the glass, they are readily reduced to elementary silver if they react with other metastable ions such as Fe^{++} and As^{+++}, which serve as electron donors.[16] The low solubility of the elementary silver so formed brings about precipitation of the metal as submicroscopic crystals. Ebell[17] was the first to point out that the yellow color of silver-stained glass is the result of metallic silver in a state of fine subdivision. The mechanism of the reduction of silver ions was first explained by Zsigmondy.[18] In order to better understand the process of silver staining, he used a transparent melt of silver nitrate and sodium phosphate in a 1:5 molar ratio as the source of silver ions. Into this melt he inserted a piece of glass and observed the formation of the yellow stain, which took place without oxygen development. He concluded that the formation of metallic silver cannot be the result of the thermal dissociation

$$Ag_2O \rightarrow 2Ag + \frac{1}{2} O_2 \ . \tag{3}$$

9

It was evident, therefore, that the oxygen must have been absorbed by a constituent of the glass. In his further research, Zsigmondy found, especially in glasses with a high FeO and As_2O_3 content, deep yellow colors, whereas glasses free from these constituents or prepared under strongly oxidizing conditions did not readily accept the silver stain. He therefore formulated the reduction process as follows:

$$Ag_2O + 2FeO \rightarrow Fe_2O_3 + 2Ag, \qquad (4)$$
$$2Ag_2O + As_2O_3 \rightarrow As_2O_5 + 4Ag. \qquad (5)$$
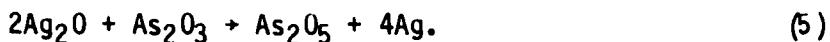
The necessity for a reducing agent to be present in the glass explains the strange sensitivity with respect to minor constituents such as sulfide, arsenic, antimony, and ferrous ions. These ions assume the role of electron donors and the Ag^+ ion that of an electron acceptor. Weyl[16] found that Ag^+ ions can also be reduced by other processes such as hydrogen treatment at 100°C, electron bombardment of the surface, cathode radiation, and X-rays. The yellowish coloration is not produced by the mere reduction of Ag^+ ions, but rather by aggregation and crystallization. During the ion-exchange process and during the reduction of silver ions into atoms, the silver atoms have considerable speed. Soon after their formation, they collide, aggregate, and form submicroscopic crystals responsible for the yellowish staining of silver-treated glasses. Under proper conditions, silver stain can be formed in all silicate glasses. The major constituents are of little influence, while minor constituents such as As_2O_3, Sb_2O_3, or FeO strongly influence the extent of glass coloration.[16] Now the question is: How is all of this related to the high losses reported to date on heavily exchanged Ag^+ ion-exchanged waveguides? The most likely answer is the following: Most researchers on this subject opted to use either commercial laboratory microscope glass slides that are generally of the soda lime category, very similar to cheap window glass, or optical quality borosilicate glasses such as BK-7. In the case of microscope glass slides, it is well known that such glasses contain considerable amounts of FeO, As_2O_3, and Sb_2O_3 as part of the constituents and are not refined of these elements in any way for obvious commercial reasons. Indeed, if one were to examine a thick bulk piece of such glasses or look at a simple microscope glass slide through its edge, a greenish-bluish color is evident, which is particularly attributable to the presence of ferrous oxide

in the sample. Optical quality glasses, as free from ferrous oxide as possible, still have a certain amount of As_2O_3 that is present intentionally in the glass. It is common knowledge to glass manufacturers that arsenic is a good fining agent added to the glass during the glass melting and preparation process to help remove bubbles and occlusions. Several mechanisms for fining are given; the most acceptable one suggests that arsenic helps reduce the oxygen concentration in the glass. At high temperatures, arsenic oxide contains mostly As_2O_3, but as the temperature is reduced, it combines with oxygen to form the pentavalent As_2O_5. The trivalent arsenic can react with the oxygen physically dissolved in the glass, reducing its concentration and shrinking the bubbles. The presence of As, therefore, is also responsible for silver reduction, even in optical quality glasses. The coloration and metallic cluster aggregations are the obvious sources and causes of high losses in the form of scattering or absorption as observed by various researchers in Ag^+ ion-exchanged glasses.

Clearly, these losses can be reduced by custom preparation of glasses free from undesirable impurities. Glass manufacturers we have contacted suggest that such customized glasses can be prepared but would be expensive, especially in small quantities, since material (high purity raw materials) and processing (fining without the use of arsenic) result in high cost. Therefore, high quality multimode waveguides produced by Ag^+ ion exchange have certain economic limitations. Commercial raw materials are inadequate if the objective is to fabricate waveguides with low attenuation on the order of a small fraction of a dB/cm.

2.1.1.4 K^+ - Na^+ Ion Exchange

K^+ is another ion that exchanges well with Na^+ ions. While a limited effort has been made thus far to employ K^+ - Na^+ ion exchange for multimode applications, this technique proves to be very useful and most promising for applications that require low numerical apertures and single-mode operation. K^+ ions diffuse in glass at a moderate pace, slower than silver but faster than thallium ions. The index increase obtained is in the range 0.006 to 0.009, and the diffusion coefficient from a KNO_3 source at 350°C in soda lime glass is about $7x10^{-11}$ cm^2/s.[9,19-23] This technique was

successfully applied to fabricate single-mode 1xN star couplers in glass substrates. Single-mode channel waveguides with typical dimensions of 4x3 μm are formed on soda lime glass slides at 350°C during a 30 min. period with a KNO_3 source. The waveguides formed are compatible with single mode fibers in regard to dimensions and numerical aperture. The propagation losses are typically < 0.2 dB/cm at 0.83 μm wavelength. For multimode operation, it is possible to extend the diffusion time and/or apply an electric field to create thick multimode guiding layers. Our experience has shown that, in these cases, the losses are even less than those for single-mode operation. The maximum index increase, however, is typically about 0.009 in soda lime or borosilicate glasses, which is lower than needed for a good match with commercial multimode graded-index fibers of high numerical aperture (NA of 0.2 to 0.3).

2.1.1.5 Tl^+- Na^+, K^+ Ion Exchange

Tl^+ - Na^+ and Tl^+ - K^+ ion exchange in glass have been used to produce light-focusing rods, planar and two-dimensional guiding layers,[9,24,25] planar microlens arrays,[26,27] and multimode star couplers.[28] As shown in Table 1, Tl^+ has the largest electronic polarizability among the monovalent ions, and therefore yields a large change in the refractive index when exchanged with Na^+ or K^+ ions. An index change of 0.1 has been observed and lower values were obtained by diluting the $TlNO_3$ source with $NaNO_3$.[24] Tl^+ is a fairly large ion and therefore has very low mobility in glass.[28] This was demonstrated by Giallorenzi et. al.[9] when no guiding layers in aluminosilicate glass were observed after an ion exchange in $TlNO_3$ melt for a period of 24 hr at 250°C. On the other hand, Izawa and Nakagome[24] were successful in producing thick guiding layers (150 μm deep) in borosilicate crown glass, but at a much higher temperature of 530°C and longer durations, reaching 72 hr. The application of an electric field considerably shortens the diffusion time. Using this method and a subsequent second exchange process to reduce the index at the surface, excellent buried two-dimensional waveguides with a near-circular profile 30 μm in diameter were formed with losses below 0.1 dB/cm.[24] For multimode purposes, this technique proves to be the most viable among other ion-exchange techniques, due to the ability to control the process inherent in the slow diffusion of Tl^+ ions and the excellent outcome of low losses and compatibility with multimode fibers.

12

The use of electrothermal Tl^+ diffusion has also been applied recently to the fabrication of planar microlens array systems.[26,27] Deep spherically symmetric index gradation was formed by diffusing Tl^+ ions through circular windows to form planar microlenses of short focal lengths. The fabrication procedure is similar to that used by Izawa and Nakagome,[24] except that a melt mixture of Tl_2SO_4 (30%), $ZnSO_4$ (40%), and K_2SO_4 (30%) was used as the dopant source at temperatures between 500°C and 600°C. The use of sulfates instead of nitrates is intended for operation at higher temperatures since nitrates dissociate at low temperatures. $ZnSO_4$ is added to lower the melting point of the sulfate mixture since each component's melting point is above the softening point of some of the glasses used. With an electric field of 7 V/mm, lenses 600 µm in radius were formed in 8 hrs. This contrasts with the formation of similar structures in 165 hrs when no electric field is applied. The same technique was recently applied to fabricate buried multimode star and access couplers compatible with graded-index optical fibers.[28]

The main problem that inhibits the wider use of Tl^+ compounds for ion exchange is their high toxicity. However, when precautions are taken and operation is maintained under proper fume hoods and controlled conditions, hazards can be reduced.

2.1.1.6 Solid-State Metallic Diffusion in Glass

In addition to ion exchange from molten salts as described above, waveguide formation in glass can also be obtained by a dry process, namely, solid-state diffusion of metallic films on glass with and without the aid of an electric field.[29-33] This process involves the evaporation of silver films about 1000 Å thick on the surface of polished glass, and subsequent diffusion at 400 to 500°C. With the absence of an electric field, deep waveguides (100 µm thick) are easily formed in a few hours. The index change in this case is very low, typically 0.001. The low index indicates slow exchange rate and low silver concentration and explains the low losses observed by such waveguides. On the other hand, with the application of an electric field of a few volts per mm, an index change of about 0.025 can be obtained.[29] In this case, higher losses and coloration are observed. As previously described,

13

silver ion reduction and aggregations are cited as the reasons for the additional scattering and absorption losses. A ten-port graded-index waveguide star coupler was reported using this method in Bk-7 glass with the help of an electric field.[33] Instead of burying the waveguides, two semicircular patterns were produced on two matching substrates, which were later aligned and epoxied together to yield a composite circular waveguide cross section. The insertion loss measured was about 6 dB.

2.1.3 Electric-Field-Assisted Ion Exchange Problems

Buried layers are necessary in guided structures for two important reasons. The first one relates to the index profile symmetry, and the second relates to the propagation losses. The profile symmetry is essential to maximize coupling between waveguides and fibers whose profile is circularly symmetric. Furthermore, by burying the guided layer below the substrate surface, a significant source of loss, namely, the surface roughness, is minimized. It is important, therefore, to consider the feasibility of the ion-exchange process for producing buried layers whose profile and geometry are compatible with those of the fibers to be used. In the ion-exchange process, buried profiles are produced by the so-called double diffusion method. This process involves exchanging the species that increase the refractive index first and then introducing a second type of species that lower the refractive index in the vicinity of the surface, yielding a graded bell-shaped profile.

For multimode operation, relatively deep waveguides are required, necessitating the promotion of the thermal diffusion with an assisting force since the speed of thermal diffusion is proportional to the square root of the diffusion time. The application of an electric field provides the additional force for driving in the exchanged ions at a faster pace, typically linearly dependent on time and electric field.

A comparison of the various ion-exchange processes is summarized in Table 2.

14

Table 2. Comparison of Various Ion-Exchange Processes

Ion Used	Index Increase Δn	Waveguide Losses dB/cm	Compatibility with Commercial Glasses	Feasibility for Fabricating Buried Layers with High NA	Fabrication Difficulties or Hazards
Li^+	f0.01	1 dB/cm	poor	poor	
Cs^+	f0.03	1 dB/cm	good	possible	toxic
Rb^+	f0.015	(high?)	good	possible	fire
Ag^+	f0.09	2 dB/cm	very poor	possible	no
K^+	f0.009	<0.2	very good	poor	
Tl^+	f0.1	<0.1	very good	possible	toxic
Ag^{+*}	f0.001	F0.2	good	very poor	no
Ag^{+**}	f0.005	F0.2	good	possible**	no

*Solid-state silver diffusion

**Electrolytic silver release. Method has been shown to be compatible with low loss single mode (low NA) waveguides. It is possible that it can be applied to large NA waveguides.

15

2.1.4 Diffusion Kinetics

Due to the low mobility of certain ions such as $T\ell^+$, an electric field may be applied across the glass substrate to assist the thermal diffusion in driving these ions at a faster pace into the glass. The extent to which the diffusion speed can be increased depends on the following: (1) electric field strength, (2) ionic mobility, (3) glass constituency, (4) temperature, and (5) ionic source concentration. All of these factors combined tend to influence the waveguide formation process, thus complicating a full understanding of the dynamics of the process, both analytically and experimentally.

Understandably, no comprehensive analysis has been reported to date that accounts for all of the above-mentioned factors and boundary conditions that influence the process.

For a planar waveguide, the diffusion is one-dimensional and is more easily treated following the diffusion theory. For an infinite doping source, the index profile follows the concentration of introduced impurities:

$$C(x,t) = C_0 \, erfc \, [\frac{x-E\mu t}{2(Dt)^{1/2}}], \tag{6}$$

where E is the applied electric field, μ is the mobility, D is the diffusion constant, and t is time. The diffusion coefficient D is defined as[34]

$$D(T) = D_0 exp \, (\frac{-\Delta E_a}{kT}), \tag{7}$$

where D_0 is the diffusion coefficient extrapolated at infinite temperatures, ΔE_a is the activation energy, and T is temperature. The mobility due to ionized impurities is given by[34]

$$\mu \simeq (m)^{1/2} N^{-1} T^{3/2}, \tag{8}$$

where N is the ionized impurity density and m is the effective mass. From Eqs. (6) through (8), it is evident that the diffusion is faster with (1)

16

higher electric field intensity, (2) higher temperature, (3) lower ionic size and effective mass, (4) lower impurity density, and (5) lower activation energy.

Unfortunately, it is not always possible to vary these parameters beyond certain limits. For example, when the electric field is increased dramatically, it will drive the Na^+ ions at a faster pace, creating a highly sodium-deficient surface layer, which, if not compensated properly, could create major network modification of the glass constituency, thus causing surface cracks and deformations. The temperature increase is limited by two factors, namely, the dissociation point of the salts used and the softening point of the glass substrate. The ionic size is dictated by the ions used. The glass constituency is also very important. The Na^+ content in the glass dictates to a large extent the index change as well as speed of both thermal diffusion and electro-diffusion, and moderately high sodium content is needed for greater exchange and increased ionic conductivity of the glass at lower temperatures. The effect of composition and Na^+ content on the net index change as well as speed of exchange was demonstrated experi-mentally.[14,35] In an experiment using Ag^+ to exchange with Na^+ ions, soda lime glass containing 12% Na_2O and TiF6 glass containing 20% Na_2O were used. The maximum index change in soda lime glass was $\Delta n = 0.1$, obtained in 1 hr at 300°C. TiF6 glass, on the other hand, generated an index change of $\Delta n = 0.22$ in only a few minutes, showing a remarkable dependence of the index change and speed of ion exchange on the sodium content in the glass.[14] The ionic source composition is also important since it modifies the effective diffusion coefficient and also affects the compensation of sodium ions drifting by the force of the electric field in the glass. Kobayashi[36] demonstrated this effect experimentally by using a mixture of $T\ell NO_3$ and KNO_3 as the salt melt source in corresponding proportions of 1:9, 1:2, and 1:1 by weight, performing the ion exchange at 450°C for 24 hrs. The diffusion coefficients of $T\ell^+$ ions in the glass were measured to be 4.34×10^{-10}, 9.8×10^{-8}, and 0.86×10^{-7} cm^2/s, respectively, indicating faster diffusion at lower $T\ell^+$ source concentration. The glass used had the following chemical composition S_iO_2 - 70 mol%, Na_2O - 15, K_2O - 2, $A\ell_2O_3$ - 1, ZnO - 6.5, B_2O_3 - 4.5,

17

and PbO-1 mol%, also determines the dissociation temperature of the salt mixture. Finally, the electrode configuration, whether metallic or insulating, as well as the distance between electrodes, tends to influence the electric field distribution and therefore the distribution or dispersion of the introduced ions.

The basic thermal diffusion process for a one-dimensional model is described by Fick's second law:

$$\frac{\partial N}{\partial t} = D \frac{\partial^2 N}{\partial x^2} , \qquad (9)$$

where N is the exchanged-ion concentration, t is time, x is the depth of penetration, and D is the diffusion constant, usually dependent on temperature and activation energy. Solving this equation yields the concentration profile

$$N(x,t) = N_0 \, \text{erfc} \left[\frac{x}{2\sqrt{Dt}} \right] , \qquad (10)$$

where N_0 is the surface concentration at the glass-melt interface. This is a simple solution that might be perturbed by several factors, such as valence difference between the exchanging ions and a change in the diffusion coefficients of the ions as they enter the medium resulting in charge accumulation. When there is no electric field across the glass substrate, the electrical neutrality in a binary exchange may be expressed as[37]

$$J_1 Z_1 + J_2 Z_2 = 0, \qquad (11)$$

where Z is the valence of the ions, J is the ion flux, and subscripts 1 and 2 refer to the exchanged ions. Assuming that the self-diffusion constants of the two ions in the glass are independent of concentration, the flux of the ions entering the glass from the melt can be written as

$$J_1 = -D_1 \left(\frac{\partial N_1}{\partial x} + \frac{Z_1 N_1 E_i}{kT} q \right) , \qquad (12)$$

where E_1 is the internal field generated by the ion exchange to equalize

18

the diffusion constants in order to maintain charge neutrality, T is temperature, and q is the electronic charge. Alternatively, the dopant flux may be written as

$$J_1 = -D_m \frac{\partial N_1}{\partial x} , \tag{13}$$

where D_m is now the effective diffusion constant defined in Eq. (2). This yields a concentration profile similar to that given in Eq. (10) with the effective diffusion constant D_m replacing the self-diffusion constant D. Therefore, the dopant concentration profile remains, but the rate of diffusion is different. When an electric field is applied, the condition for charge flow under the electric field is

$$J_1 + J_2 = J \tag{14}$$

when both ions are monovalent, i.e., $Z_1 = Z_2 = 1$. Assuming that the self-diffusion coefficients are concentration-independent, then J_1 and J_2 are given by

$$J_i = -D_i \left(\frac{\partial N_i}{\partial x} + \frac{N_i E_T}{kT} q \right), \quad i = 1,2. \tag{15}$$

where E_T is now the total electric field (internal and applied). The index profile may now be obtained from the flux equation as

$$n(x,t) = n_s + \frac{\Delta n}{2} \left[erfc \left(\frac{x - \mu E_T t}{2\sqrt{Dt}} \right) + exp \left(\frac{\mu E_T x}{D} \right) erfc \left(\frac{x + \mu E_T t}{2\sqrt{Dt}} \right) \right] \tag{16}$$

From this equation, it appears that an electric field will produce a higher index at a given depth x for the same diffusion time. The diffusion speed is also dependent on the magnitude of the field. A change in the profile shape is also evident from the exponential term modifying the complementary error function.

2.1.5 Two-Dimensional Confinement Distortions

One of the important issues relating to the successful fabrication of circularly symmetric multimode channel waveguides in glass by the electric-

field-assisted ion exchange is the tendency for the dopant ions to diffuse sideways.[38,39] An example of this effect was demonstrated experimentally by Lilienhof et al.[39] The authors used a diluted melt of $AgNO_3/NaNO_3$ with 10 mol% $AgNO_3$ as the exchanging source in borosilicate glass (DESSAG type D263) and soda lime glass (VERTEX). Their substrates were very thin (0.3 to 0.5 mm thick), and their masking waveguide openings were relatively wide (35 to 106 μm). The masking materials used were Ti, Pt, SiO_2, and Si_3N_4, all yielding similar results. The anode used was the salt melt, and the cathode was a gold film evaporated on the back of the sample. Buried layers were formed by a subsequent exchange in pure $NaNO_3$ after removing the original masks. Their study demonstrated the development of side lobes and a sideway diffusion especially for wide channels. The side lobes were more evident when the mask opening was large (>40 μm). The side diffusion and depth after diffusion were found to be somewhat nonlinear with exchange time for a given electric field intensity and temperature. Narrower windows were found to yield deeper penetration and to have slightly more side diffusion for a given diffusion time.

The side diffusion effect was also observed in very narrow (single-mode) waveguides when silver ion exchange was used.[40] The effect was manifest by cream-colored bands along the waveguide sides. Walker et al.[40] attributed this effect to electrolytic deposition of metallic silver beneath the edge of a conducting aluminum mask. Such an occurrence was not observed when an insulating (anodized Aℓ) mask was used. Their explanation of this phenomenon follows Doremus' suggestion[1] that an electrical potential exists between an ion exchanger and the solution or melt with which it is exchanging, as a result of thermodynamical activity and mobility differences. Since more Na^+ ions diffuse out of the glass than Ag^+ diffuse in (under no electric field), the glass becomes under a negative potential with respect to the melt. An electrochemical potential may also exist between the conducting mask and the melt, leaving the mask under an additional negative potential with respect to the melt. When the two voltages are different, ionic current flows, thus accelerating the Ag^+ indiffusion and retarding the Na^+ outdiffusion. Since the ion exchange is a one-to-one process, the excess indiffused silver will be reduced and deposited beneath the conducting mask edges, which also affects the net

20

index change. It should be noted that the results of Walker et al.[40] correspond to narrow single-mode channel waveguides, and no external electric field was used in the diffusion process.

Wilkinson and Walker[38] studied the effect of the masking film (conducting on nonconducting) on the ionic concentration gradient of very narrow Ag^+ ion-exchange waveguides in glass under no external field by solving the diffusion equation under two masking conditions, metallic and nonconducting. They postulate that when a metallic mask is used, the electrostatic boundary condition on the metal mask requires that the electric field be zero. This implies that the gradient of the silver ions be zero at the mask-glass interface. The width of the diffused region is reduced, and the central section of the diffused region shows more curvature. It should be noted again that the case considered by the authors assumed very narrow (3.5 μm wide) waveguides under no fields.

When very wide multimode channel waveguides were fabricated with an external electric field as in the Lilienhof[39] study, the side lobes were not attributed to differences in chemical potentials between the melt and the masking material, as suggested by Walker et al.[40] No difference in the profiles was observed when different masking materials were used, conductive and insulative.[39] It is not easy to draw a conclusion between the two results. However, it is reasonable to argue that when an external electric field is applied, which is usually larger than the electrochemical fields, the mask-induced fields may be overwhelmed by the external fields, yielding similar results for conducting and nonconducting masks, especially for very wide openings.

2.2 Apparatus for the $Tl^+ \rightarrow Na^+$ Ion-Exchange

The $Tl^+ \rightarrow Na^+$ ion-exchange experiments were conducted in a Lindberg "lift top" vertical furnace which was slightly modified for use under a fume hood. The glassware, shown in Figure 1 consists of a long flat bottomed quartz tube which rests on the bottom of the furnace and extends up above the furnace rim. A standard ground quartz joint connects a cap to
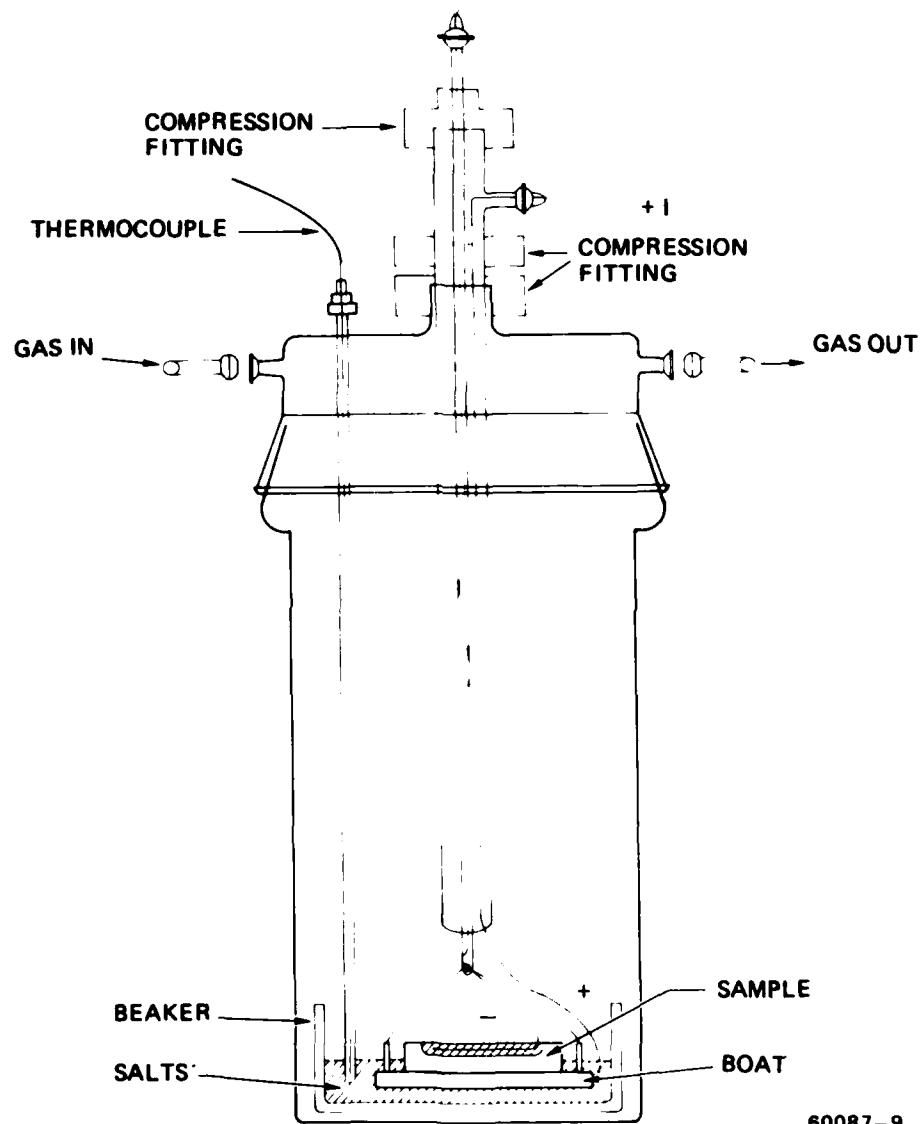
Figure 1. Apparatus for the $Tl^+ - Na^+$ ion exchange under an electric field.

the top of the tube. There are four feedthroughs in the cap. Two are standard 1/4" ID tubing for gas flow. The third has a compression fitting which is used to insert a sealed long quartz tubing containing a thermocouple for temperature monitoring. The fourth feedthrough is located in the center of the cap and fitted with a compression fitting to allow a double-hollow quartz tubing-rod (used to load the sample) to slip fit through the opening. The compression fittings allows random height positioning of the thermocouple and sample holding rods. The double hollow in the central tubing accommodate two electrically isolated platinum wires used to apply the electric field and carry the electrical current. These wires are sealed at the top of the double hollow tubing, and connected with external wires to the power supply through ball joints.

A quartz beaker in the bottom of the tube contains premeasured impurity salts. This beaker is lined with a stainless steel beaker (not shown in Figure 1) to isolate the molten salts from spilling into the main tube when the quartz beaker breaks for some reason. A quartz boat with a rectangular opening is used to hold the glass sample. The boat has four protruding rods used to attach platinum wires to the boat and sample.

The operation of the setup is as follows: The back-etched glass sample is loaded face down onto the boat outside the chamber. The boat is then tied to the lift rod through platinum wires. The platinum cathode wire is firmly placed in the back-etched depression, and a small amount of salt is placed on it in the depression. The sample and holder are lifted and lowered carefully into the vertical tube. The sample is then lowered to a position slightly above the surface of the salt source in the bottom beaker. The thermocouple tubing is similarly positioned. The furnace is allowed to warm up till the salts melt (500-600°C), during which the temperature is recorded on a chart recorder. Argon is allowed to flow through the vessel throughout. When ready to perform the E-field assisted diffusion, the sample and thermocouple are lowered into the melt. Electric field is applied with a dc power supply, and the current is recorded on a chart recorder. After the diffusion is complete, the sample and thermocouple are lifted above the melt surface, and the furnace is turned off and allowed to cool down to room temperature.

When cold, the sample is lifted out, and rinsed well with water along all exposed glassware, fittings etc. Extreme caution is taken at this time to avoid skin contact with the components exposed to the toxic salts.

2.3 Choice of Materials

Several factors determine the proper choice of materials including impurities, substrates, and masking materials. These factors are:

1. Sample optical quality
2. Sodium and potassium content (glass conductivity)
3. Sample softening temperature
3. Temperature of operation and time
4. Salts and their melting and decomposition temperatures
5. Masking materials

Furthermore, the materials and parameters chosen must be capable of achieving the following:

. 1. Low transmission loss
2. Relatively high NA (large Δn)
3. Reasonably short diffusion times

The general guidelines are, therefore;

1. To get low loss waveguides, use high transmission optical quality glass, commercially available, with sufficient Na content. BK-7 and soda lime are good possible choices. BK-7 is probably better as will be seen later.
2. To get low loss and high NA waveguides, $T\ell$ is the better choice for the impurity.
3. To perform the diffusion in reasonably short time, operation must be at relatively high temperatures (500°C-600°C) since the diffusion of $T\ell$ is slow.
4. Operation at high temperatures requires the glass to have a relatively high softening point. Soda lime glasses in general, have low softening points.

24

5. For the same reason, the salts must have high decomposition temperatures. This favors the use of sulfates over nitrates, which decompose and boil above 400°C.

6. The sulfate's melting points are relatively high (600-800°C) and must therefore be lowered by the addition of other impurities from compatible salts such as zinc salts.

7. The masking film must be compatible with photolithographic techniques and be able to sustain no deterioration by oxidation or chemical reactions with the salts at high temperatures.

From these guidelines, it seems like BK-7 or a comparable optical quality glass which is commercially available is the proper choice. The sulfates also emerge as the better choice for several reasons including high decomposition point, and viscosity. Nitrates usually creep over the sample sides rapidly causing short circuits due to their low viscosity. Gold and SiO_2 are appropriate choices for the masking film due to their low reactivity with the salts. Details of the observation found with the salts, glasses, and masking materials will be given later in this report.

3. STAR COUPLER MASKING CIRCUIT DESIGN

The waveguide and coupler mask design was comprehensive to allow for the evaluation of the waveguides as well as couplers at the same time. Various initial waveguide widths are introduced to determine the effect on the final diffused guide width. Furthermore, the mask allows one to study the effect of the mixing region in the 2x2 and 4x4 couplers on the output power distribution uniformity. The designs are shown in this section. For the 2x2 couplers, two configurations are employed as shown in Figure 2. In the upper configuration (a), the structure consists of two Y-branching waveguide sections connected together with a short straight channel referred to as the mixing region, having the same width as the other waveguides in the Y-junctions. Configuration (b) with a mixing width twice the width of the two entering waveguide was expected to yield a constant waveguide crosssection throughout the length of the glass sample, thus conserving the number of modes throughout. Each design is repeated for different widths ranging from 5 μm to 30 μm in increments of 5 μm at a
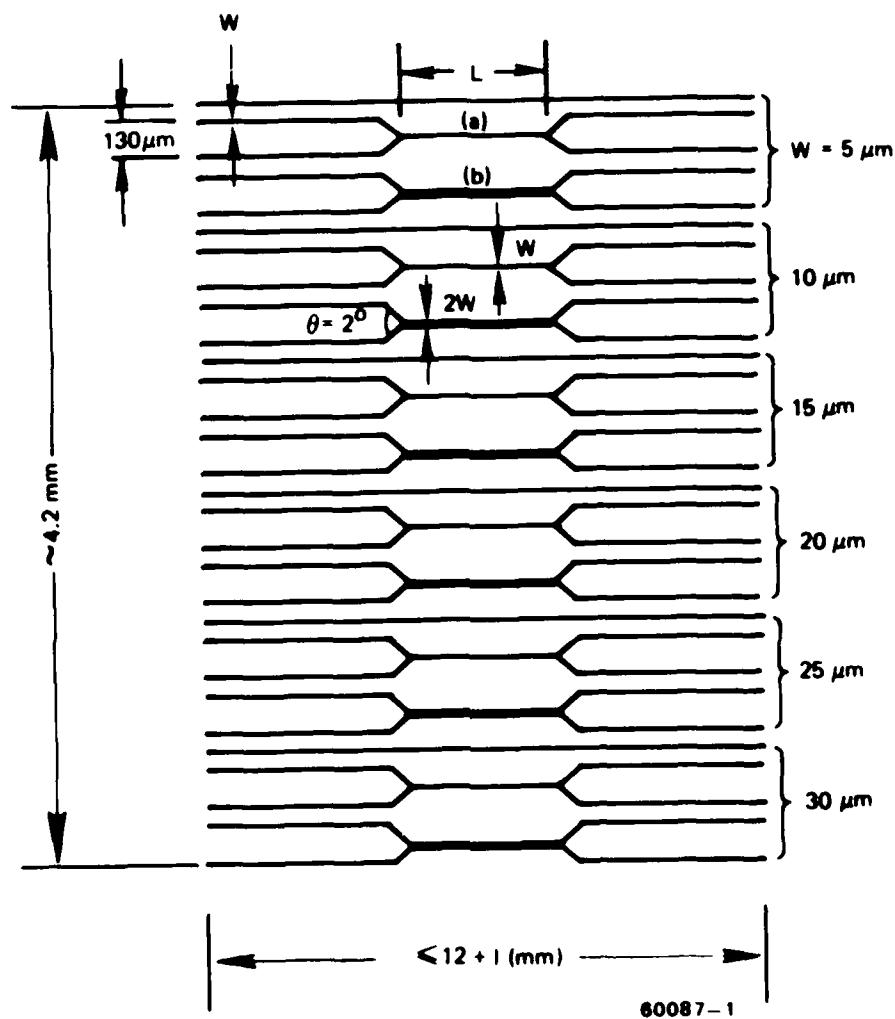
Figure 2. Mask layout for the 2x2 waveguide couplers.

time. Each family of variable width structures is repeated three times for three different mixing region lengths of 5, 10, and 15 mm. The branching angle of the Y-junctions is kept at 2°. Straight channel waveguides of corresponding widths interface between the various structures. The center to center spacing between the input and output channel pairs of the 2x2 couplers is kept at 130 μm.

Figure 3 illustrates the designs for the 4x4 couplers. Three geometries are used in this case. The first (a) combines two input ports at a time through Y-junctions and proceeds to combine through another Y-junction to a central mixing region. The output is branched out through similar 1x2 Y-branchings yielding 4 output ports at the end. The widths of all guides is maintained throughout. The second geometry (b) is similar to the first, except for doubling the channel width at every Y-emerging branch, thus yielding a central mixing region whose width is four times the width of the input or output branches. In the third configuration (c), all four input and output branches merge simultaneously into the central mixing region whose width is four times the width of the input or output channels. Again, configuration (c) with a mixing width four times the width of the four entering waveguides was expected to yield a constant waveguide crosssection throughout the length of the sample thus conserving the number of modes. The subsequent experiments showed configuration (c) to perform the best in distribution uniformity and low loss.

All patterns are repeated six times for channel widths of 5μ, 10μ, 15μ, 20μ, 25μ, and 30μ, respectively. A straight channel with a corresponding width is included with each set of three coupler patterns. Each set is further repeated three times for mixing region lengths of 5 mm, 10mm, and 15 mm in order to determine the appropriate mixing region length. The branching angle is set at 2° throughout. The center-to-center spacing between the adjacent input and output ports is kept at 130 μm. The patterns are interfaced with straight channels of corresponding widths for evaluation and comparison purposes. A V-groove alignment pattern is also included on the same mask with a center to center spacing of 130 μm, which corresponds to the center to center distance between the adjacent channels at the input and output ports of the star coupler patterns throughout.
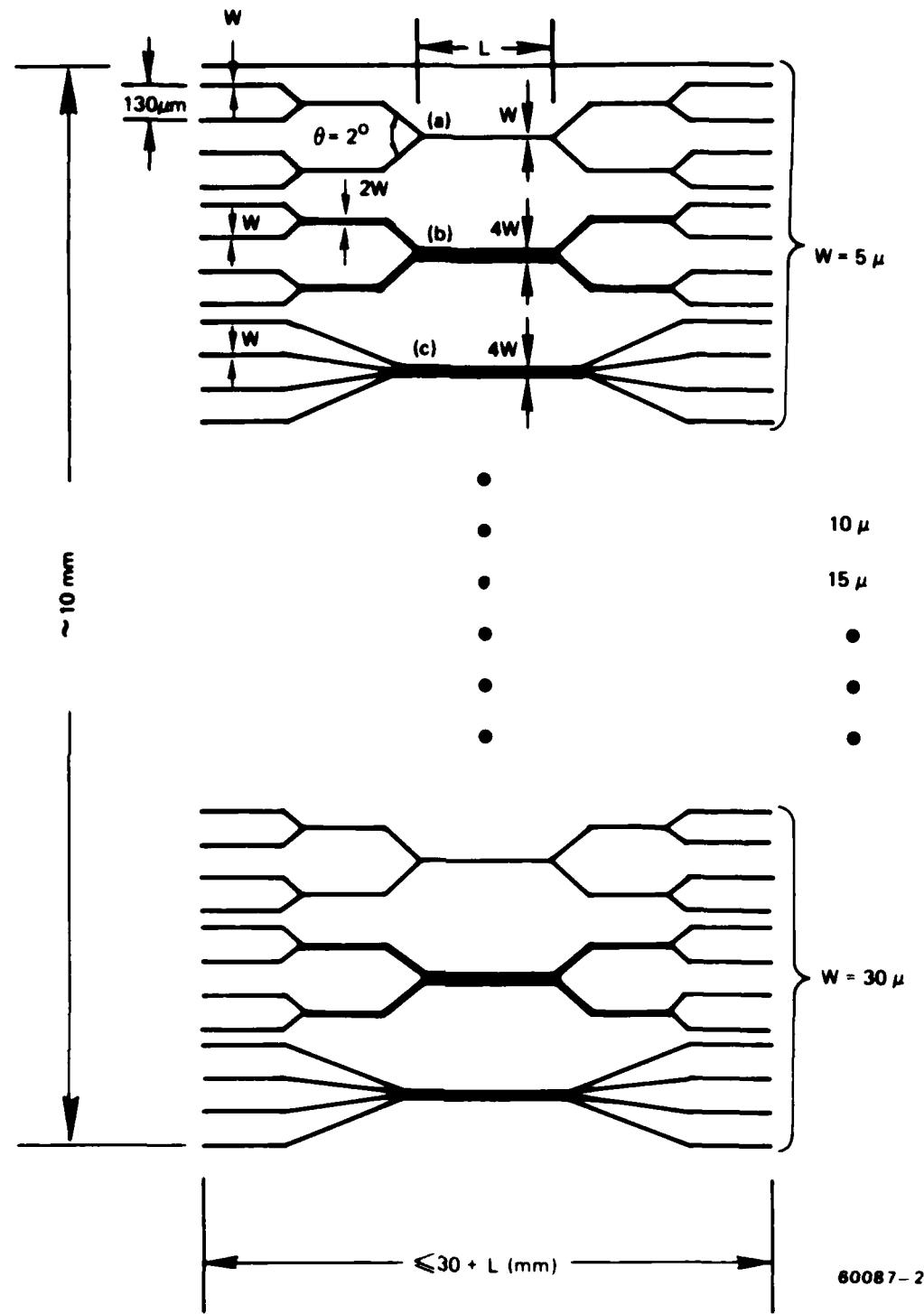
27

Figure 3. Mask layout for the 4x4 waveguide couplers.

This spacing is adequate for alignment of an array of commercial multimode fiber with 125 µm O.D.

An overall layout of the various features on a 4" x 4" chrome plate is illustrated in Figure 4. The various patterns are situated such that all patterns, (2x2) or (4x4), can be delineated on the BK-7 sample which is typically 0.75" wide. A copy of the mask in Cr oxide was also made available.

4. WAVEGUIDE CIRCUIT FABRICATION

4.1 Sample Preparation :

The BK-7 samples were procured with typical dimensions of 0.75"x0.75"x3", polished on four sides, and ground only on the two square ends. The purpose for having much of the surfaces polished is to avoid or delay molten salt creeping and short circuits. The sample height was chosen to be 0.75" for the same reason. The procedure for sample preparation and processing is illustrated in Figure 5. The sample is first covered with parafin wax on all sides. A slit is opened through the wax at the back surface and the wax removed. The sample is then immersed in HF or buffered oxide etch in a stirred basin to etch away a depression (2-3 mm deep) where the glass is exposed on the back side. The wax is removed thereafter and the sample is chemically cleaned afterwards.

A proper masking film is deposited over the front surface by E-beam evaporation. Films of Cr (10000 A), Au/Cr (5000/300 A), SiO_2 (5000 A), SiO_2/Cr (5000/300 A), Pt/Cr (3000/300 A) , and Au/Ti (5000/300 A) were attempted with varied results. After deposition, photo-resist is spun over the coated surface. A special fixture was made to accommodate resist spinning at 4000 RPM due to the large size and weight of the sample. Resist UV exposure was carried out either on a mask aligner or a UV printer. Again the sample size presents certain logistical problems when standard mask aligners are used. After exposure and development, the pattern is etched away either by wet or dry etching, or both. After cleaning, the sample at this point is ready for loading into the ion exchange chamber.

V − GROOVE PATTERN, 130μm CENTER TO CENTER

2 x 2, L = 5 mm   W = 5−30 μm, ΔW = 5 μm

2 x 2, L = 10 mm   W = 5−30 μm, ΔW = 5 μm

2 x 2, L = 15 mm   W = 5−30 μm, ΔW = 5 μm

4 x 4, L = 5 mm   W = 5−30 μm, ΔW = 5 μm

4 x 4, L = 10 mm   W = 5−30 μm, ΔW = 5 μm

4 x 4, L = 15 mm   W = 5−30 μm, ΔW = 5 μm

60087−8

Figure 4. Overall layout of the 2x2 and 4x4 chrome mask plates.

30

a) SAMPLE, POLISHED
   ALL SIDES

d) TURN UPSIDEDOWN
   SiO_2 DEPOSITED

SiO_2

INDENT IN
WAX ONLY

b) WAX COATING, BACK
   SIDE SLOT OPENING

e) PATTERN
   DELINEATION

60087—6

c) HF ETCHING

ETCHED GROOVE
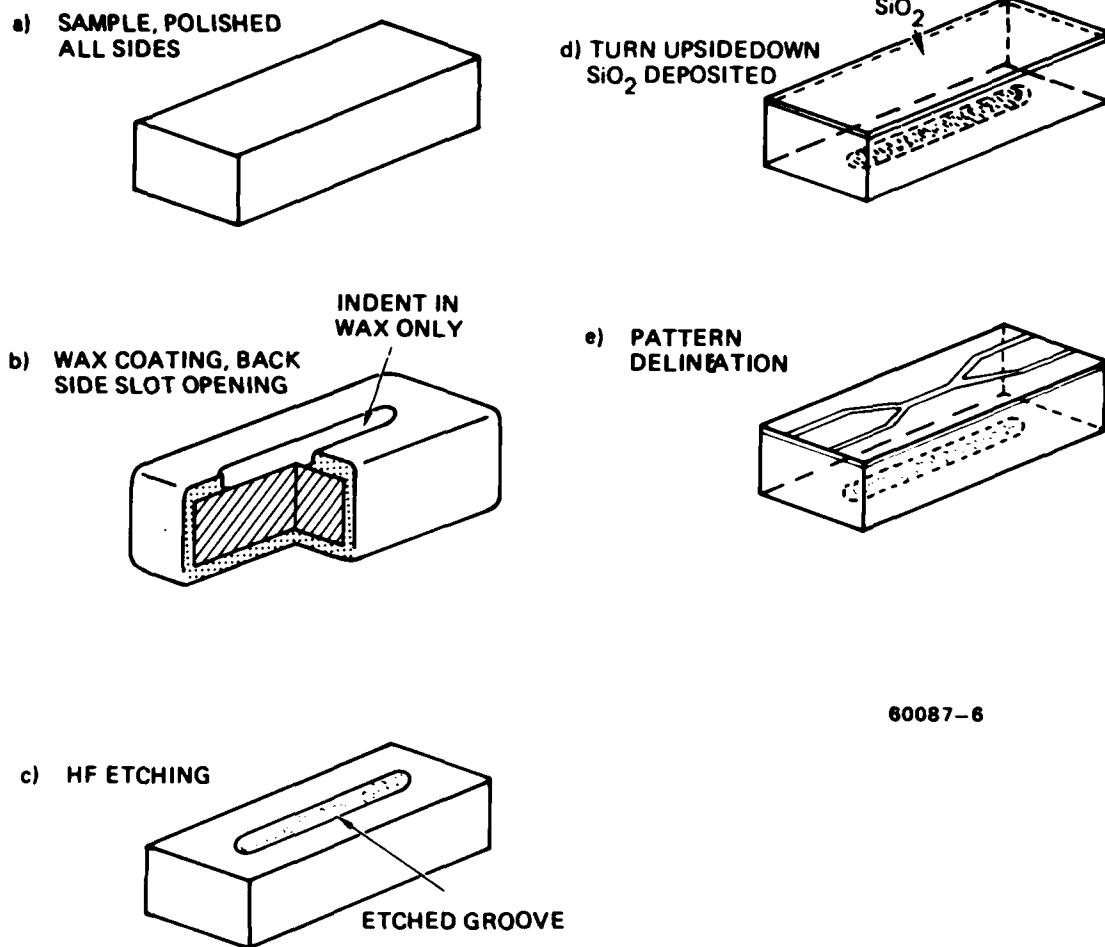
Figure 5.   Procedure for glass sample preparation.

31

4.2 $T\ell^+$ Waveguide fabrication

The following salt mixture was used for the waveguide impurity source:

$T\ell_2SO_4$	30% wt %
K_2SO_4	15% wt %
Na_2SO_4	15% wt %
$ZnSO_4$	40% wt %.

Sufficient amounts were used to allow the sample to submerge slightly less than half way. While each of these chemicals has a melting point greater than 588°C, the combined mixture melts at approximately 500°C. This mixture was first melted and left to mix and interdiffuse for a few hours. Loading the samples and connecting the setups was explained in Section 2.2. The procedure for waveguide fabrication is illustrated in Figure 6. After loading the sample and bringing the furnace to 540°-560°C, the sample is lowered into the melt. The electric field is applied and the flowing electrical current is monitored and recorded on a chart recorder along with temperature. Typical fields applied were in the range 7-10 V/mm, yielding typical currents into the substrate in the range 50-150 mA depending on temperature and the height of the salt solution with respect to the sample sides. To create 30-50 μm deep surface waveguides, 30-60 minutes of $T\ell^+$ electro diffusion is sufficient at a temperature of 550°C at an electric field of 7-10 V/mm in BK-7 glass. Attempts to inject higher current by using higher fields were counter-productive since the additional electrical heat caused fractures and strains leading to sample breakage.

After the first diffusion step, the masking film was removed and the samples were cut and edge polished for surface waveguide evaluation. The cuts made usually overlapped the ends of the depression in the back of the sample. In order to carry a second electro-diffusion to bury the surface waveguides, a new back depression had to be created. This was done by cutting the back of the sample to a flat, thus removing the old depression. A new depression is formed by waxing and etching using the same procedure described earlier.

1. SiO$_2$ MASKING FILM EVAPORATION

SiO$_2$ FILM
GLASS

2. PHOTOLITHOGRAPHIC PATTERN DEFINITION

PHOTORESIST

3. FILM ETCHING

4. FIELD ASSISTED ION EXCHANGE

Tl$^+$ SALT

5. MASKING FILM REMOVAL

SURFACE WAVEGUIDES

6. WAVEGUIDE BURYING

Na$^+$ SALT

7. BURIED WAVEGUIDES
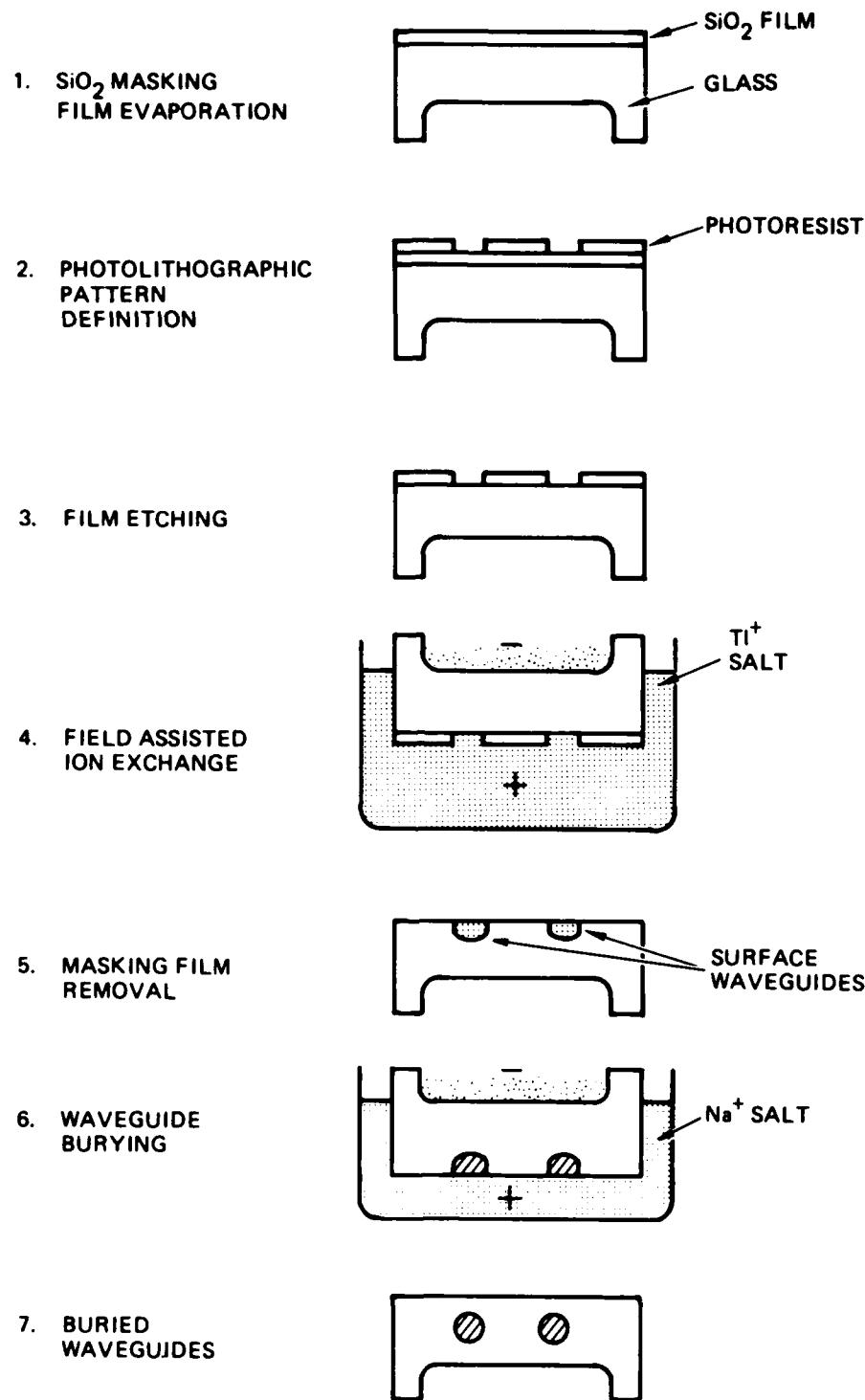
60087-7

Figure 6.   Procedure for waveguide fabrication.

33

Alternatively, after all the fabrication parameters are optimized, there is no need to cut the sample after the first diffusion step. In this case, the masking film is etched away, and the sample is reloaded for the second diffusion step.

The purpose of the second electro-diffusion step was to bury the waveguide so that surface losses due to potential surface contamination could be minimized. During this program the mixture used to bury the waveguides was: $ZnSO_4$, 50 wt %; Na_2SO_4, 30 wt %; K_2SO_4, 20 %. The potassium was included to obtain a well-behaved molten mixture. However, examination of the buried waveguide couplers near the end of this program indicates that potassium may have contributed to increased scattering.

4.3 Problems Encountered

It is instructive at this point to describe some of the problems encountered during this program and their solutions.

1. _Glassware breakage_: This was a problem frequently encountered during all phases of the program, causing undue delays. The components subject to frequent breakage were the salt fused quartz beaker and the quartz boat. Since both are nonstandard items, one has to keep adequate supply since procurement and availability consumed time. These items broke frequently during the cooling down period when the molten salts recrystalized, causing tensions and strains within the beaker and quartz boat. Standby supplies were not always available, and some delays were encountered because of this problem.

2. _Masking film_: Several masking films were attempted in order to choose the best film that withstands the chemical reactions with the salts at high temperatures. The combinations tried include: Cr, Al, Cr/SiO_2, Pt/Cr, Ti, Au, Cr/Au, Ti/Au, and SiO_2. Al and Ti were found to oxidize (forming high index planar waveguides) and thus become difficult to etch afterwards; this necessitated surface polish for oxide removal, which is not an easy task without damaging the surface region. Cr surprisingly reacted with the salts and was found to

34

degrade rapidly. Even 1.5 μm thick Cr did not survive more than 0.5 hr at 550°C. The reaction appeared also to degrade the salts. Pt and Pt/Cr were attempted but were found difficult to etch during pattern definition due to substantial uncontrollable undercut. Gold survived nicely but had an adhesion problem and tended to flake off. Au/Cr adhered and survived well, but the thin Cr layer still caused undesirable reactions at the openings where the Cr edges where exposed. Au/Ti also survived, but the thin Ti layer oxidized (evidently getting the oxygen from the glass) and was thus difficult to remove.

SiO_2 survived best and yielded the cleanest surfaces with no degradation to the surface and no reaction with the salts. The only problem with SiO_2 is etching since the chemical wet etchants also attack the glass. Etching the SiO_2 with a dry CVD plasma process avoided this problem and yielded the best results. The process of finding a good masking film compatible with the process consumed a large fraction of the program time but this mask was necessary for the successful completion of this program.

3. <u>Trapped air bubbles</u>: In the early designs of the boat (sample holder), tne opening in the boat is about the size of the sample surface. Accordingly, when the sample is placed on the boat and immersed into the molten salt, bubbles were trapped in the boat hollow under the sample. These bubbles could not escape easily due to the meniscus effect and the high viscosity of the sulfates. This caused non-uniform diffusion since different surface areas were not uniformly exposed to the melt. To avoid this problem, new boats were designed such that the opening width is sufficiently larger than the sample width. In this case, the sample rests on the boat surface at its ends, leaving the sides free of contact with the boat to allow the bubbles to escape.

4. <u>Slow warm-up time of the furnace</u>: A substantial portion of the diffusion tube (especially the cap and fittings) protruded beyond the rim of the furnace heating chamber. This coupled with the large

35

diameter ($\sim$ 5") and short height of the heating element ($\sim$ 10") did not provide good thermal isolation and substantially slowed the warm-up time. For example, it takes about 6 hours for the furnace to reach 550°C. Such a long period causes logistical problems to the operator, thereby decreasing the number of possible experiments.

5. <u>Health and safety issues</u>: Needless to mention, there are some hazards imposed by $T\ell$ compound processing. Because of the health and safety considerations, processing techniques have been necessarily modified. Considerable care must be taken with the molten thallium salts due to the potential for inadvertent leaks at high temperatures. The investigator was warned that he may not stick his head into the hood to look inside the chamber. Problems of this nature were impediments in fully investigating, trouble shooting and remedying problem issues.

4.4. Waveguide Characteristics

From our thermal $T\ell^+ - Na^+$ ion-exchange (no electric field) experiments, an approximate value of the diffusion coefficient was determined following the relation:

$$D = \frac{d^2}{4t} \tag{17}$$

where D is the diffusion coefficient, d is the diffusion depth (1/e) and t is the time. For Bk-7 at 560°C, the diffusion coefficient was approximately 2×10^{-15} m^2/sec. It took, for example, 30 hrs. to diffuse a waveguide 35 μm deep at 560°C without an electric field. A similar penetration depth was obtained in less than 1 hour, with the application of an electric field of 7 V/mm at the same temperature using the same salt mixture:

|	
$T\ell_2SO_4$,	30 wt %
Na_2SO_4 ,	10 wt %
K_2SO_4 ,	10 wt %
$ZnSO_4$,	50 wt %

4.4.1 Side Diffusion

For two dimensional waveguides (patterned with SiO_2 mask), side diffusion was evident in both thermal and electric field assisted ion-exchange processes. Figure 7 summarizes that the side diffusion (on each side) increases as the initial width is decreased. The depth measured at the center of the waveguide behaves similarly. In narrower waveguides, the cross-section of the waveguide after the first ion-exchange was nearly semicircular. For shallow waveguides (< 5 μm deep), especially for wider waveguides, the waveguide cross-section exhibited swelling on both sides which penetrated deeper than the central region as was observed by Lilienhof et al.[39] Such waveguides were of no interest to us since the depth and aspect ratio were not compatible with the objectives.

4.4.2 Thermally Diffused Waveguide Couplers

Our investigation has shown that thermally diffused thallium waveguides (without electric-field-assistance) are exceptionally good with very low scattering. Figure 8 shows cross sectional microscope photograph of a 4x4 coupler (sample #3) fabricated thermally with no electric field. The waveguide was backlighted with a tungsten lamp for the photograph. The exact pattern to be seen in the microscope depends upon the sample illumination. Only a first diffusion was performed on this waveguide. The duration of the thermal ion exchange was 3 hours at a temperature of 570°C. The melt mixture for the first diffusion was described above. The waveguide center to center separation is 130 μm. The mask opening in Figure 8a is 5 μm and the opening in Figure 8b is 20 μm. Side diffusion of thallium results in the half moon shaped cross section with dimensions of ~50 μm wide and 25 μm deep. The thallium concentration is highest near the surface of the glass. The swelling of the waveguide is due to the larger size of the Tl^+-ion than that of the Na^+-ion which it replaces.

Thermal diffusion over a longer period of 22 hrs formed excellent waveguides with minimal surface scattering. Figure 9 shows a crosssection microscope photograph of a thermally diffused thallium (single diffusion) waveguide coupler (sample #8). The sample was thermally diffused for 22 hrs at 570°C. The thallium concentration gradient does not appear to be as
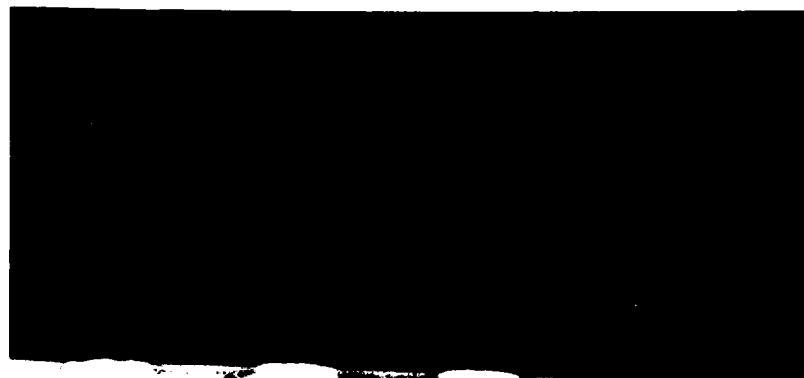
37
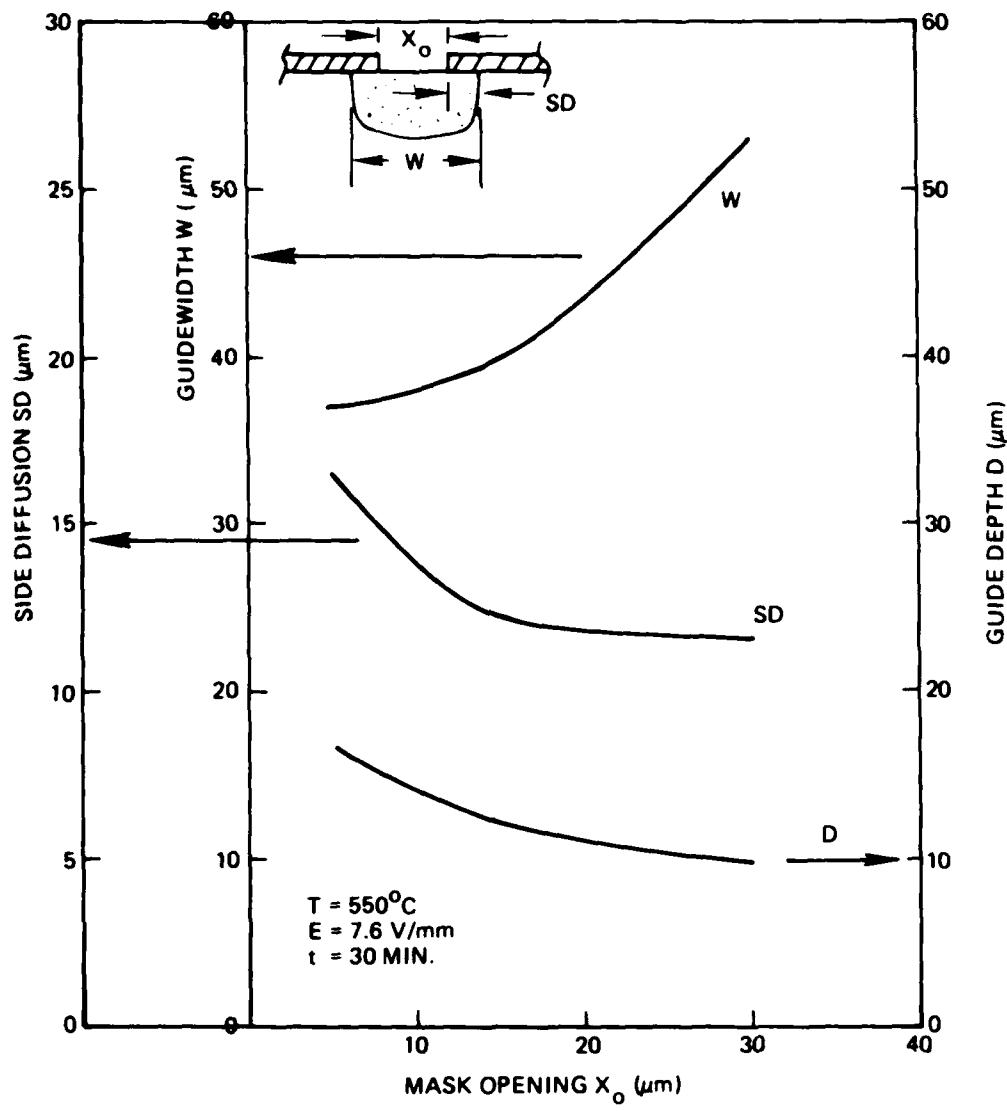
Figure 7.   Waveguide side diffusion, width, and depth as a
function of waveguide mask opening.

60087-4

38
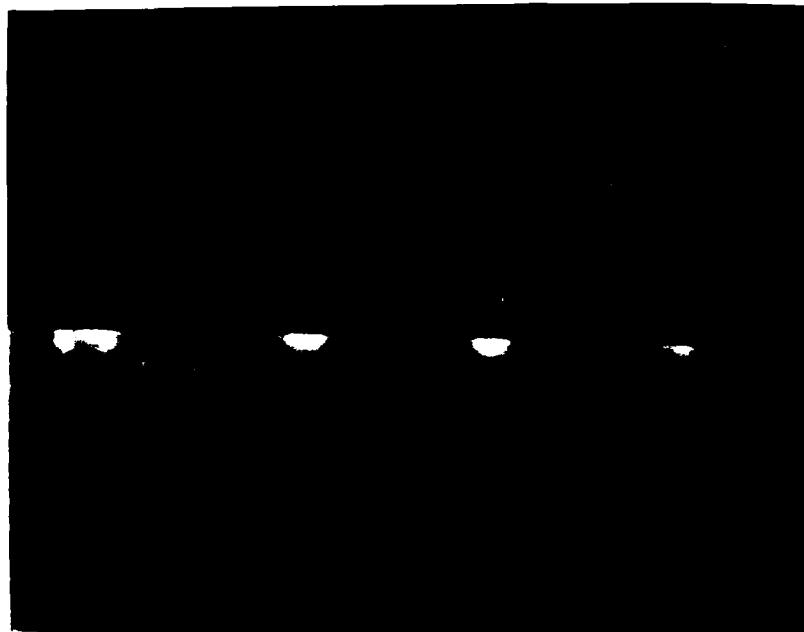
Figure 8. Cross-sectional microscope photograph of a 4x4 coupler (sample #3) fabricated thermally (with no electric field). First diffusion only. 3 hour duration, T=570°C, (a) 5 μm mask opening (b) 20 μm mask opening.
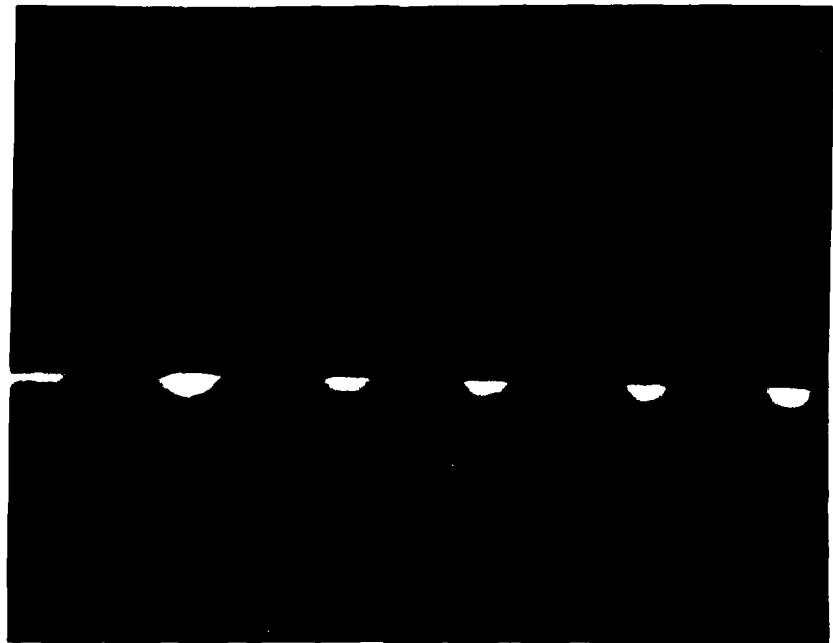
39

Figure 9. Cross-sectional microscope photograph of a 2x2 coupler (sample #8) fabricated thermally. 22 hours at 570°C.

high as that for waveguides with shorter diffusion run.

4.4.3 Waveguide Couplers with Thermal First Diffusion and Electric-Field-Assisted Second Diffusion

A 2x2 coupler (sample #6) was fabricated with a second diffusion performed to bury the waveguides. The first diffusion was done thermally without an electric field; the diffusion duration was 8 hours at 560°C. Figure 10a shows the cross-sectional microscope photograph after the first diffusion, Figure 10a. A swelling of the waveguide is clearly seen. The halo around the most intense portion of the waveguide may be due to potassium diffusion. As described previously, the potassium was included in the diffusion melt during the investigation of mixtures and their melting temperature. The molten mixture behaved well. (The mixture had not been changed during the latter part of this program.)

Subsequent burial of the thallium waveguide was attempted with an electric field assisted diffusion for 2 hours where the molten mixture contained only sodium, potassium and zinc sulfates. The electric field was again 7.2 V/mm, resulting in a steady state current of 120mA at 570°C. The waveguide coupler cross section after the second diffusion is shown in Figure 10b. Considerable swelling of the waveguide surface is to be noted. The photograph indicates that partial burying of the waveguide has been attained. The burying process, however, resulted in considerable optical scattering in the waveguide. We believe that the second diffusion with an electric field has driven the more mobile Na^+- and K^+- ions through the less mobile Tl^+- ion waveguide in a non-uniform way, modifying the smoothly changing refractive index of the waveguide obtained after the first thermal diffusion.

During the fabrication of samples #5 to #11 after SiO_2 was found to be the best masking material, a lack of an immediate supply of thallium sulfate from commercial suppliers forced us to reuse old mixtures. A small quantity of the original mixture was added to the old mixture. Our supply of thallium was depleted beyond expectation by glass breakage and by the study of masks. Vendors were unable to supply us with a new stock of thallium sulfate until the end of the program. The excessive use of the

41
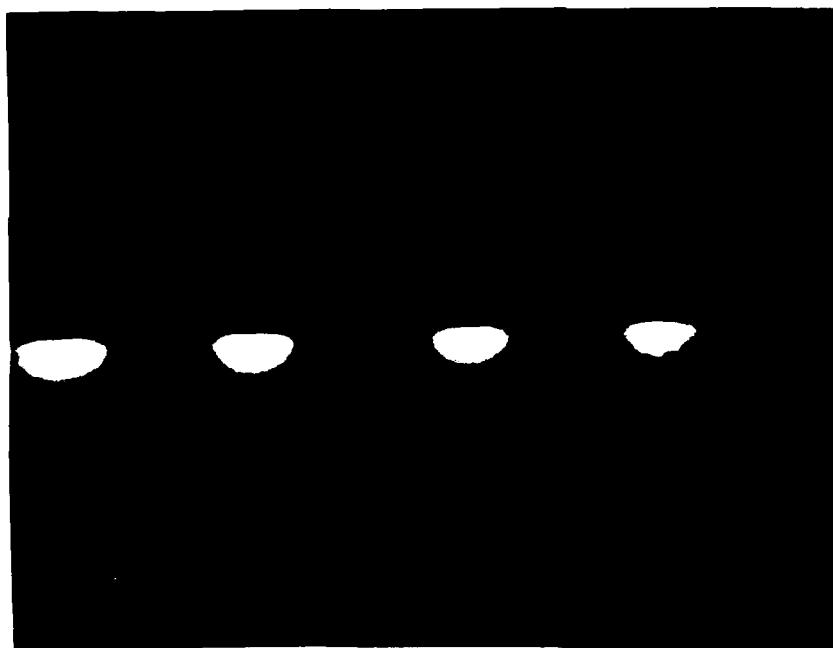
Figure 10. Cross-sectional microscope photograph of a 2x2 coupler (sample #6) double diffused. (a) thermal diffusion for 8 hours, (b) electric field assisted second diffusion for 2 hours.

old mixtures as well as the potassium impurity during the first diffusion, may have contributed to the excess scattering.

4.4.4 Electric-Field-Assisted First, Second, and Third Diffusion

A 2x2 waveguide coupler was fabricated with electric field diffusion. Then two attempts were performed to bury the couplers with electric-field-assisted diffusion initially for 1 hour, then for two hours.

Figure 11a shows a cross-sectional microscope photograph of a single electro-diffusion 4x4 coupler (sample #5) corresponding to the largest mask opening of 30 μm. No photo was taken of the section with a smaller opening. An electric field of 7.2 V/mm was applied during the electro-diffusion which resulted in a steady state current of 120 mA at the melt temperature of 570°C. The duration of the diffusion was 27 minutes, after which the electric field and the furnace electric current were turned off abruptly. The sample was then pulled up just above the melt to cool down gradually in the furnace. The optical transmission of the sample after the first diffusion was qualitatively examined. The optical throughput distribution of the electric-field-assisted first diffusion surface waveguide couplers was well behaved but showed a slightly larger amount of scattering than a thermally diffused (~25 hours) thallium waveguide coupler.

The same sample after a second electric field assisted diffusion is shown in Figure 11b. This photograph is of a different part of the sample where the mask opening was 5 and 10 μm. The second diffusion was done in a mixture of sodium, potassium and zinc sulfate in an attempt to "bury" the thallium enriched waveguide, as described above. The SiO_2 mask was removed for the second diffusion. Some swelling of the waveguide is evident as the thallium ions drift further into the glass. Again an electric field of 7.2 V/mm was applied, resulting in a steady state current of 120 mA at a melt temperature of 560°C. The duration of the second diffusion was one hour. The sample was removed and examined qualitatively for its optical characteristics. Considerable scattering from the waveguide was evident in

43

Figure 11. Cross-sectional microscope photograph of a 4x4 coupler
(sample #5) after electric field assisted diffusions.
(a) First diffusion, 27 minutes (30 μm mask) (b) second
diffusion, 1 hour (5 and 10 μm mask) (c) third diffusion,
2 hours (5 μm mask).

44

the near field output pattern.

Figure 11c shows the microscope cross section photograph of the same #5 sample after a third diffusion to further bury the thallium-enriched waveguide. Again, an electric field of 7.2 V/mm was applied, resulting in a steady state current of 120 mA at 560°C. The duration of the third diffusion was 2 hours. The photograph suggests that the refractive index gradient near the surface is not as high as in Figure 11b, leading to the conclusion that the very high thallium concentration at the surface has been depleted. The photograph shows a considerable amount of index inhomogenieties which can lead to poor waveguide characteristics. Examination of the optical transmission of the coupler after the third diffusion, indeed, exhibited a considerable degradation of the optical throughput with an excessive amount of scattering. Illumination of one arm of a coupler also resulted in excitation of the adjacent couplers. Further details of the optical transmission properties are described in the next section.

5. TESTS AND EVALUATION

In this section, the test procedures are described and the test results are given for the numerical aperture, measurements of losses, output coupling uniformity, and coupling efficiency to commercial multimode fibers.

5.1 Numerical Aperture

The numerical aperture was measured by exciting the input of the waveguide with all the possible modes it can support and measuring the conical angle of the optical beam from the output of the waveguide. For this measurement to be a good representative of the actual numerical aperture, the waveguide must be saturated with all the modes it can support. To do this, the laser beam is expanded with a beam expander, and the input to the waveguide is focussed with a high NA lens such as 40X or 60X magnification. A screen is placed at a relatively long distance (ℓ) from the output facet of the sample (say 0.5-1.0 m) without an output lens

as shown in Figure 12, and the radius (r) of the spot on the screen is measured. The numerical aperture is:

$$NA = \frac{r}{(r^2 + \ell^2)^{1/2}} = \sin\theta \qquad (18)$$

Alternatively, the same measurement could be done by replacing the high NA input lens with a multimode fiber, which in turn, is excited to saturation (steady state) with all the modes it can support. Our measurements using both methods yielded numerical aperture of 0.23 for a waveguide approximately 50 μm deep. This particular waveguide was fabricated with a mixture consisting of: Tl_2SO_4 , 40 wt%; Na_2SO_4, 15wt%; K_2SO_4, 15 wt% and $ZnSO_4$, 40 wt%. It is estimated that the Δn of the waveguide is approximately 0.017 following the formula:

$$NA = \sqrt{2n\Delta n} \qquad (19)$$

where n is the refractive index, and Δn is the index increase. The numerical aperture measurements by the method described above can be performed on a single channel waveguide only. Overlapping of the outputs from the output channels of the 2x2 and 4x4 couplers does not allow accurate NA measurement by this method.

The numerical aperture of sample #5 (see Figure 11) was measured to be ~0.11, well below the value of 0.23 mentioned above. The long thermal process had diffused the thallium particularly near the surface concentration, thereby reducing the Δn. Generally, a second diffusion sample exhibited a smaller NA than a first diffusion sample.

5.2 Transmission Losses

The transmission losses are separated into two parts, namely, the losses incurred in a straight channel waveguide, and the total loss of the coupler. This way the excess circuit loss could be identified and may be used in the future to further optimize the guided circuit designs.

The transmission losses were measured by the end-fire coupling method. The test setup is shown in Figure 13. It consists of a He-Ne

46

SCREEN

INPUT
LIGHT

WAVEGUIDE
OUTPUT

2r

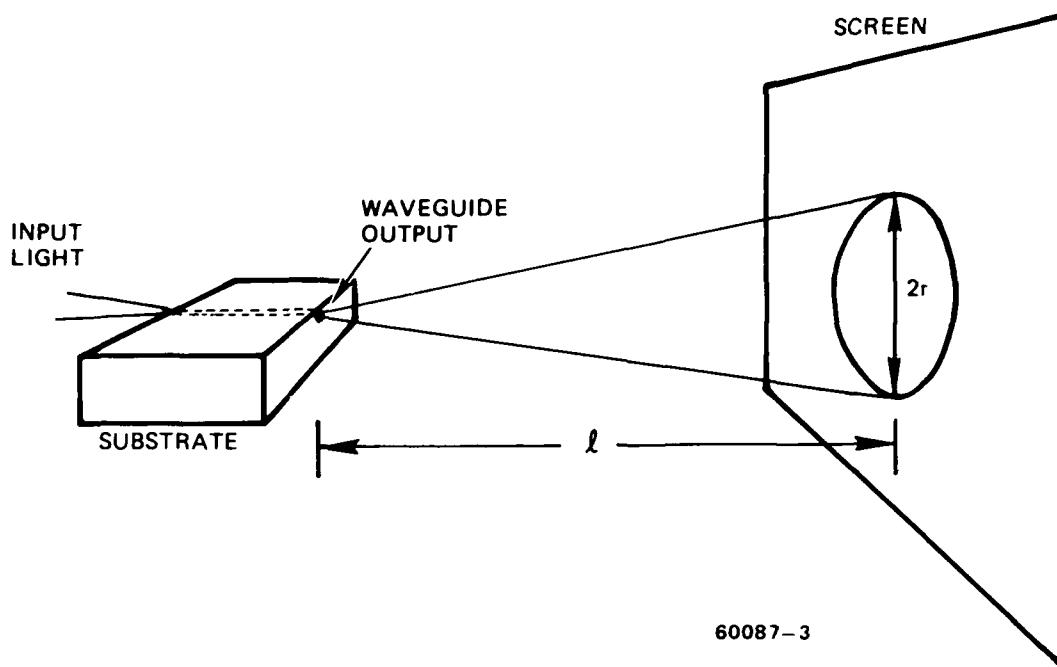SUBSTRATE

ℓ

60087-3

Figure 12.   Method for measuring the numerical aperture of a single
channel.

laser, a beam splitter, a beam expander, two microscope objectives (one used to focus the beam onto the waveguide, and the second used to image the output of the waveguide), a detector, and a chart recorder. The beam expander and iris were adjusted so that the focussed beam approximately matched the NA of the waveguide. Precision alignment stages with XYZ $\alpha\beta\theta$ degrees of freedom are used to align the polished sample for maximum coupling efficiency. With the sample removed, the optical power is measured by bringing the two lenses in and focussing onto the detector. This value P_1 represents the input power. With the sample in place and after aligning and maximizing the coupling efficiency, the output power P_2 is measured. This output power contains loss components attributable to the waveguide loss α, the Fresnel reflections (FR), and the coupling efficiency η, such that:

$$10 \log \frac{P_2}{P_1} = \alpha + F R + \eta \qquad (20)$$

The Fresnel reflections from the two facets of the sample are easily calculated to be ~ 0.37 dB for glass. Since the focal spot of the input lens is much smaller than the waveguide cross-section, η can be considered zero (100% input coupling) if the numerical aperture of the focussed beam is smaller than the numerical aperture of the waveguide. From this assumption the waveguide loss can be determined after accounting for the Fresnel reflections. All other losses in the optical setup cancel out since they are the same when P_1 and P_2 are measured. The beam splitter is used to account for fluctuations in the laser output. Our best results yielded a straight channel waveguide attenuation of <0.1 dB/cm. For a device 5 cm long, the overall loss is 0.5 dB.

To measure the overall coupler losses, the same procedure is used. In this case, the input power is focussed on one of the input channels. The output is measured by adding the total power of the output channels. This is done by scanning the detector and recording the power from each output port. The overall losses measured for 2x2 and 4x4 first diffusion couplers (after accounting for Fresnel reflections) were < 1.0 dB and < 1.4 dB, respectively. The 2x2 coupler was 3 cm long, while the 4x4 coupler was 5 cm long. From these measurements, and referring to the attenuation in a

48
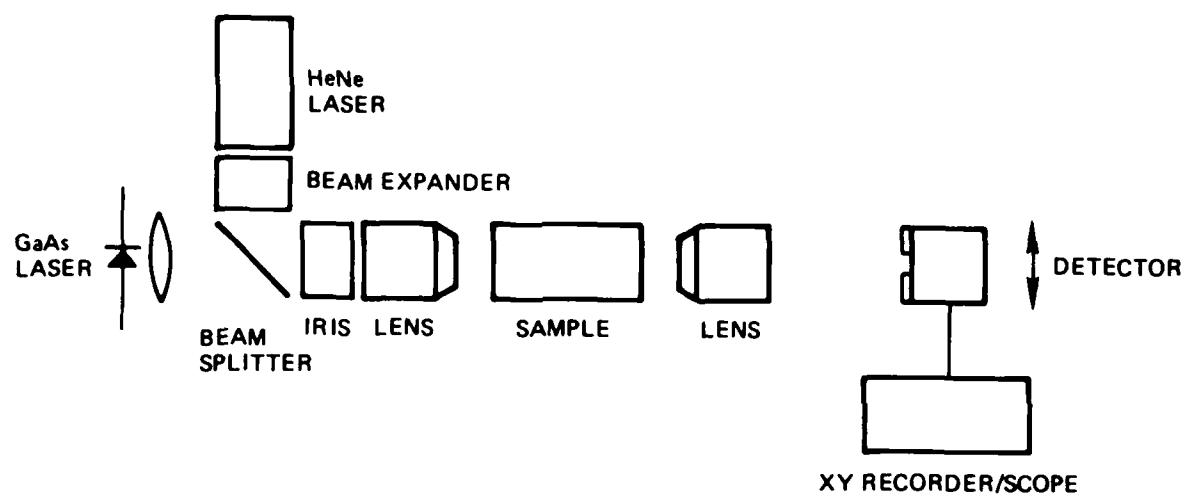
Figure 13. Transmission test set-up for measuring, insertion loss and optical power distribution of the coupler.

straight waveguide of approximately 0.1 dB/cm, it appears that the excess loss encountered by the 2x2 coupler is < 0.7 dB, and by the 4x4 coupler is < 1.0 dB.

5.3 Output Power Distribution

The output power distribution of a 2x2 single diffusion coupler, a 4x4 single diffusion coupler and a 2x2 double diffused coupler is described in this section. A HeNe laser beam was expanded, focussed and end-fire coupled into each input port of the edge polished sample. The output was imaged with a second lens and focused through a circular iris to a detector. The output power of each output port. was measured and recorded for each input port. The output power was also displayed on an oscilloscope by scanning the output across the detector iris with a scanning mirror.

The output scan of a 2x2 coupler (sample #8) fabricated with a single thermal diffusion for 22 hours at 570°C is shown in Figure 14a. The coupler mask opening was w=5 μm and the mixing length was L=15 mm and had a width of 2W=10 μm. The total outputs of both ports were compared with the throughput of a straight channel (with mask width w=5 μm) located adjacent to the 2x2 coupler on the glass substrate. The scan of the straight channel is shown in Figure 14b. The ratio of the total output of the coupler for each input port and the output of the straight channel is shown in Figure 14c.

The chart in Figure 14c shows the fractional output distribution of channel ports 1' and 2' as a function of input ports 1 and 2. The variation is less than 0.2 dB. The total output is compared with the output of the straight channel in the chart. The variation in total output of the coupler is 0.8 dB. The throughput ratio indicates that no significant loss is incurred by the 2x2 coupler.

Figure 15 shows the power distribution of a single diffusion 4x4 coupler (sample #3) which was fabricated by thermal diffusion for 3 hours at 570°C. This sample was described in section 4.4.2 and Figure 8. Scans of the output as a function of the input ports is shown in Figure 15a. The
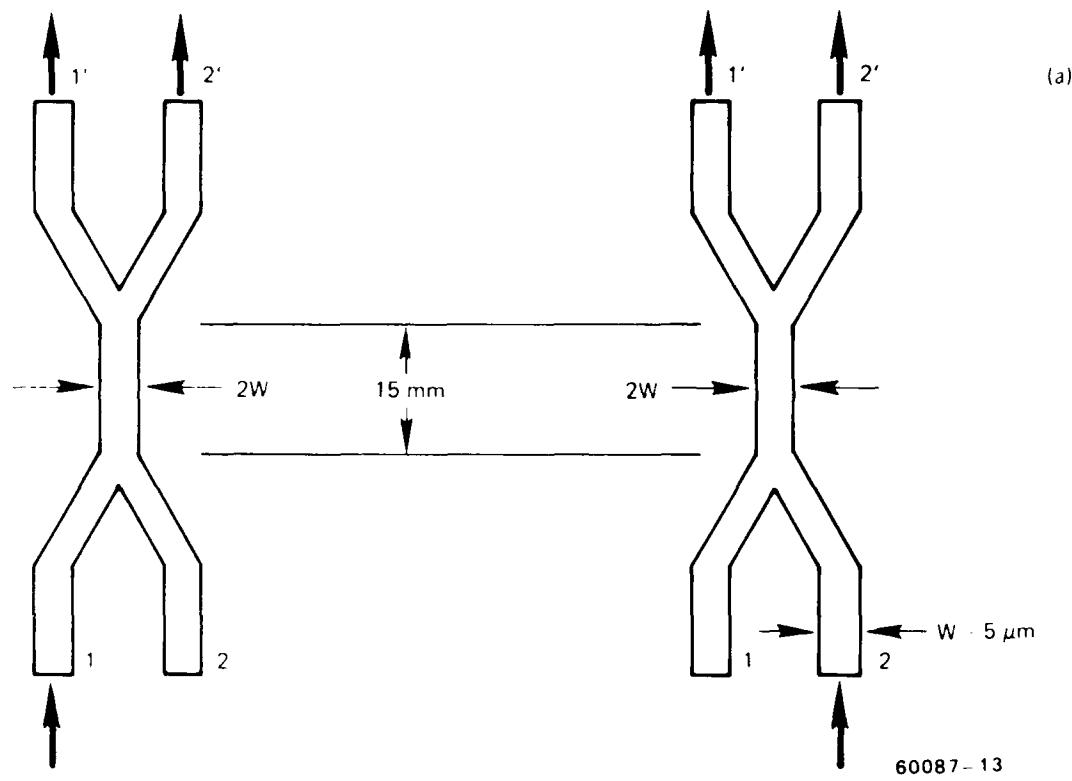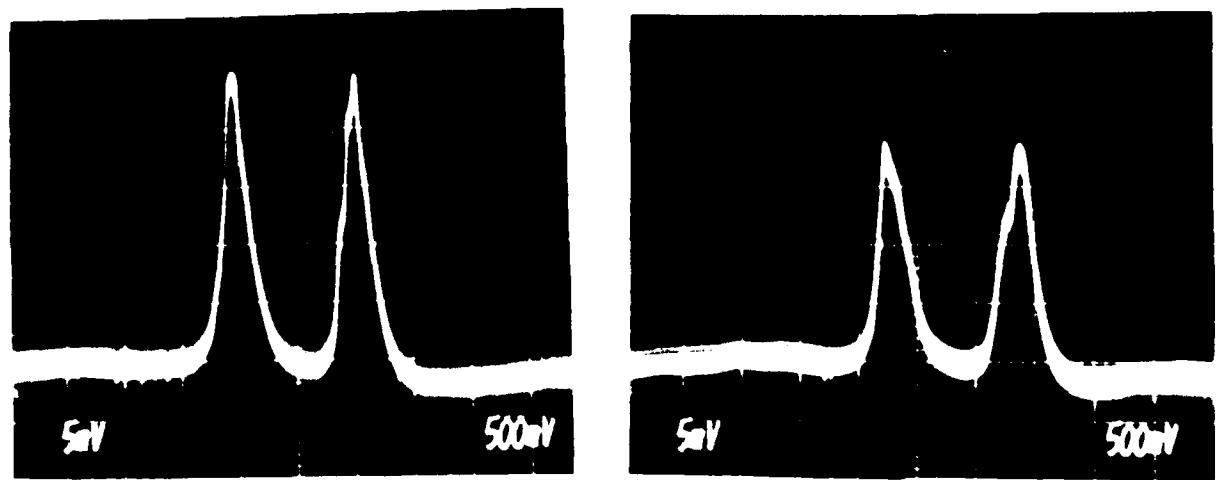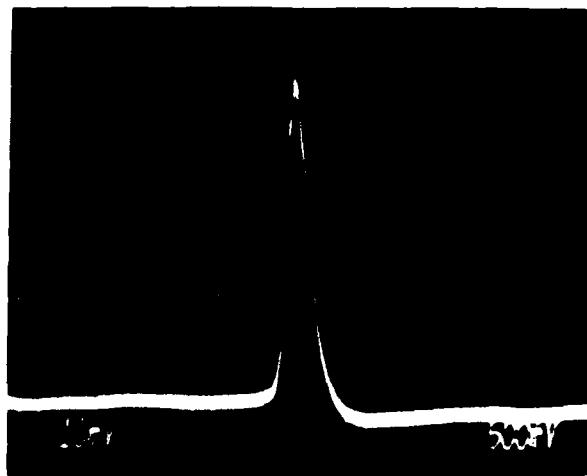
50

Figure 14. Coupler output power distribution of a 2x2 coupler
            (sample #8).
            (a) output power scan

(b)

OUTPUT INPUT	1'	2'	THROUGHPUT RATIO (COUPLER/ST. CHANNEL)
1	0.51	0.49	1.02
2	0.49	0.51	0.85

(c)

60087-10

Figure 14. (b) output scan of a straight channel
(c) splitting power ratios and throughput ratios
for total coupler output to single channel
output.

output scan of corresponding straight channel located next to the coupler is shown in Figure 15b.

The output distribution chart of the 4x4 coupler is shown in Figure 15c. The fractional outputs of each output port are shown for a given input port; the output power variations about the mean ranges from .6 to 2 dB. The throughput ratios of the total coupler outputs to the straight channel output varies from -.6 dB to -1.5 dB. The output power distribution variation is probably much higher than desirable for a multimode coupler. However, these results are for a thermally diffused sample fabricated near the end of the program after the masking problems were solved. Much better distribution can be expected as this ion-exchange technology improves.

Figure 16 shows the power distribution of a double diffused 2x2 coupler (sample #6) described in section 4.4.3 and Figure 10. The first diffusion was done thermally for 8 hours, the second was an electric-field-assisted diffusion. Figure 16a and b shows the scan patterns of the coupler and Figure 16c that of the corresponding straight channel. The output variation of the coupler is shown in Figure 16d; the variation about the mean is <0.4 dB. The throughput ratio is fairly large for one of the coupler input, corresponding to ~ 3.5 dB. We found that most of the couplers on this double diffused sample showed a significant amount of inconsistencies not observed on singly diffused couplers. At this time we believe that the deterioration of performance of the second diffusion couplers arose from the inclusion of potassium in the mixture, the difference in ion mobilities of thallium, potassium and sodium, and the long period required to "bury" the thallium waveguide.

5.4 Mixing Lengths, Widths and Geometry

The effort of mixing lengths and widths were examined semi-quantitatively on the numerous first diffusion couplers fabricated on this program. For the 2x2 and 4x4 couplers we found that a couplers with mixing lengths of 15 mm performed better than the couplers with mixing lengths of 5 and 10 mm. The distribution of output power was found generally to be

53

a)
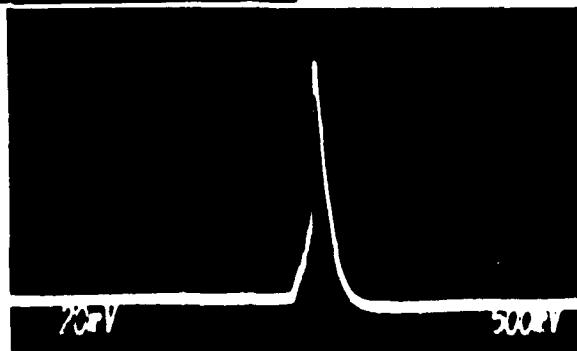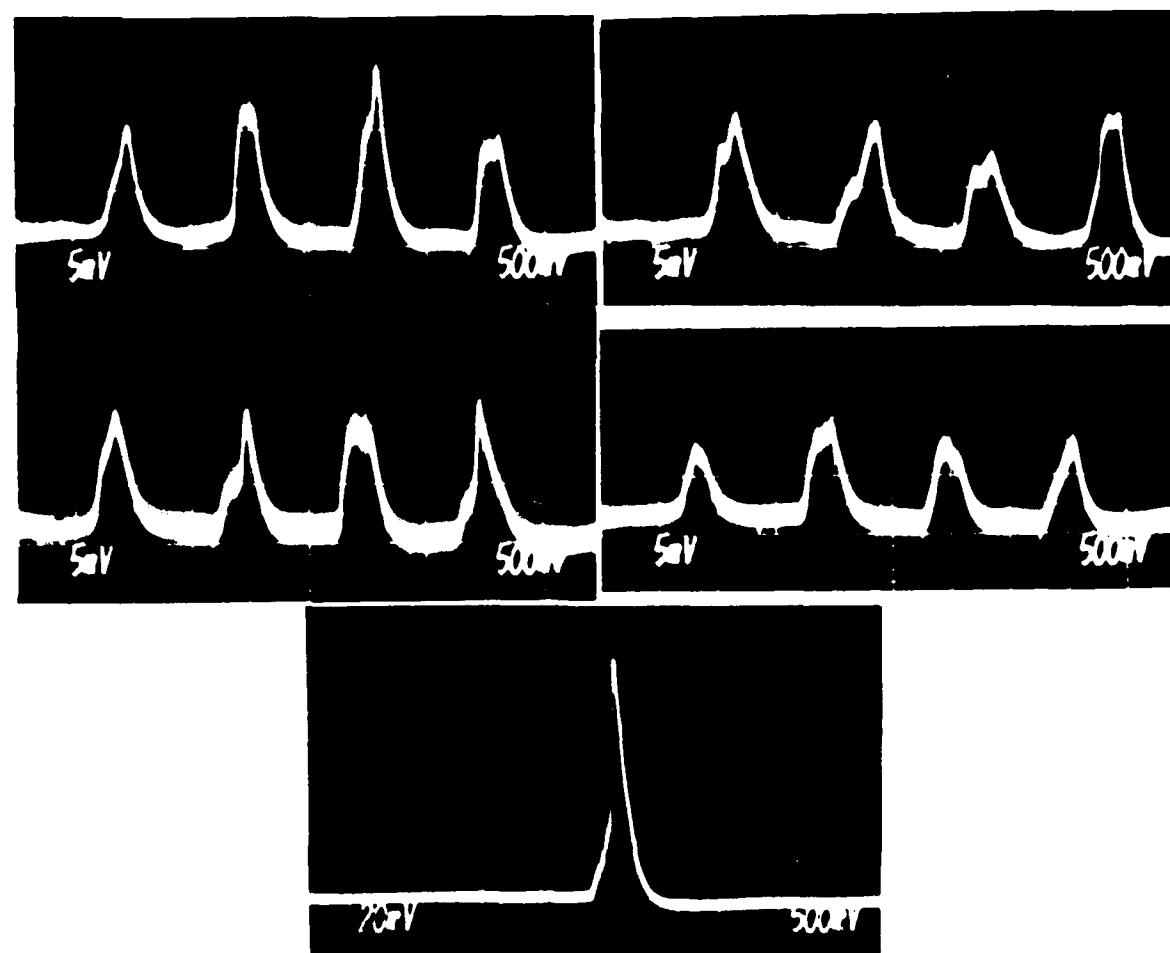
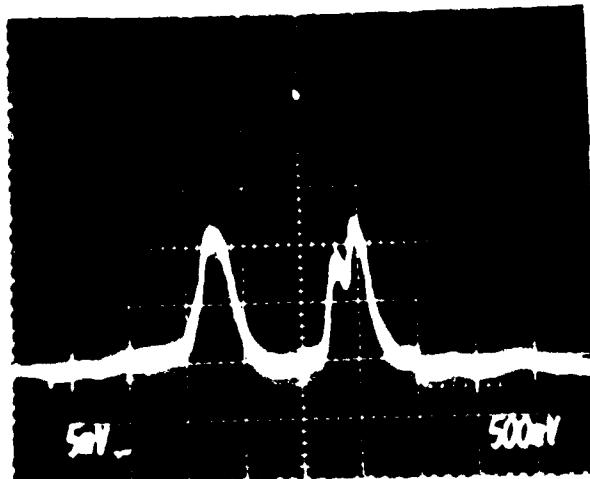| OUTPUT INPUT	1'	2'	3'	4'	THROUGHPUT RATIO (COUPLER/ST. CHANNEL)
1	0.38	0.35	0.18	0.20	0.74
2	0.21	0.35	0.23	0.21	0.71
3	0.25	0.28	0.25	0.22	0.88
4	0.32	0.25	0.18	0.25	0.80

60087−16

c)

Figure 15. Coupler output power distribution for a 4x4 coupler (sample #3). (a) output scans of 4x4 coupler (b) output scan of single channel (c) power output ratios and throughput ratios for total coupler output to single channel output.

54

OUTPUT INPUT	1'	2'	THROUGHPUT RATIO (COUPLER/ST. CHANNEL)
1	0.47	0.53	0.72
2	0.52	0.44	0.44

d)

60087 14

Figure 26. Coupler output power distribution for a 2x2 coupler
sample #2, 'a' and 'b' output scans of coupler,
'c' scan of straight waveguide, 'd' power of output
ratios and throughput ratios.

more uniform for the longer mixing lengths. This was more evident, as expected, for the 4x4 than the 2x2 couplers.

The best widths for the mixing region, again for output uniformity and higher power output, was 2W for the 2x2 coupler (when W is the single channel width) and 4W for the 4x4 couplers. We also examined two different geometries for the 4x4 couplers and found that the "single star" (where all ports were connected directly to the mixing region) configuration resulted in the best output uniformity.

5.5 Final Waveguide: New Mixture Without Potassium

A new mixture not containing K_2SO_4 was used to fabricate the final and best waveguide (sample #13) for this program. The mixture was: 36 wt% of thallium sulfate, 21 wt% of sodium sulfate and 43 wt% of zinc sulfate. A new shipment of thallium sulfate received near the end of this program was used. The 2x2 coupler was fabricated with an electric-field-assisted diffusion. Diffusion parameters were: 30 minute diffusion period, an electric field of 7.2 V/mm, electric current of 120mA, and a diffusion temperature of 575°C.
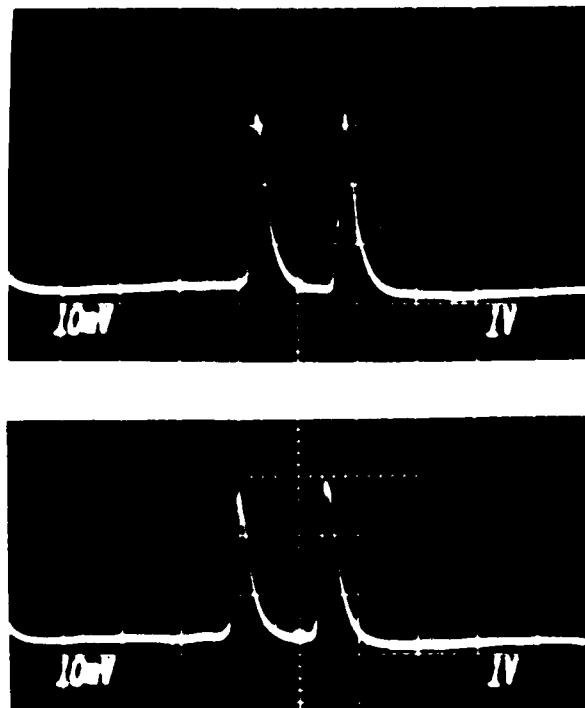
A cross-section miscroscope photography of a pair of 2x2 waveguide couplers is shown in Figure 17a. Again, the waveguides were backlighted through a pinhole with a tungsten lamp. The photograph shows a fairly smooth variation of the light intensity. A definite swelling of the waveguide is noted, again due to the larger thallium ions replacing sodium ions. The mask opening for the waveguide in Figure 17a was 15μm. The mixing lengths of both couplers were 15mm. The waveguide width is measured to be ~35μm and ~18μm deep. The scanned outputs of one of the couplers is shown in Figure 17b. The coupler output distribution is shown in Figure 17c. The output variation about the mean is < 0.1 dB.

The numerical aperture of a straight channel waveguide on this sample was measured with the method described in Section 5.1. The horizontal WA was ~0.19 and the vertical NA was ~ 0.20.

Sample #13 fabricated with a new mixture, not containing potassium, exhibited the best waveguides in the cross sectional photograph of all the

56

(a)

(b)

OUTPUT INPUT	1'	2'
1	0.49	0.51
2	0.49	0.51

(c)

60087-18

Figure 17. Final 2x2 waveguide coupler (sample prepared with a new
mixture (no potassium)).
(a) cross-sectional microscope photograph
(b) 2x2 coupler scan output, (c) power output ratios.

57

first diffusion waveguides fabricated during the program. The very low scattering of this sample and the excellent distribution of the couplers clearly indicates that very good thallium couplers can be fabricated with electric-field-assisted ion diffusion. What remains is further experiments to bury the waveguide.

6. CONCLUSION

The efforts of this program focussed primarily on developing and implementing techniques for fabrication low loss integrated optical multimode waveguides in glass by the $T\ell \rightarrow Na^+$ electric field assisted ion exchange method and using such methods to construct 2x2 and 4x4 star couplers. The results show that very low loss (< 0.1 dB/cm) waveguides can be fabricated on glass by this method. The experiments show that potassium should not be included as a mixture component. The results also show that monolithic optical waveguide circuit structures such as passive star couplers can also be fabricated yielding promising results for future development. The technical difficulties encountered in a limited laboratory environment are not limiting factors for the future. The issue of toxicity can be dealt with under a controlled environment. Other logistical problems such as apparatus and equipment can easily be modified and designed to optimize yield. The process itself is compatible with volume production as it can be envisioned that a large number of couplers for example can be simultaneously fabricated in a batch process. There are, however, few areas of further research and development that are worthwhile looking into in the future. They include:

1. Investigation of glasses other than Bk-7 containing larger amounts of sodium whereby the ion-exchange can be done faster at lower temperatures. If this can be done the issue of salt mixture melting point compatibility with the softening point of the glass as well as the durability of the masking film become easier to deal with. This suggests the use of nitrates instead of sulfates for example.

2. Investigation of masking film durability and integrity due to

58

chemical reactions with the salts at high temperatures. While SiO_2 was found compatible with the process, it presents, nevertheless, a problem during the removal of the masking film in preparation for the second diffusion stage for waveguide burying. Surface polishing is not a desirable approach, and chemical etching attacks the glass. Dry etching works, but it also attacks the exposed glass surface to some extent. Operation at lower temperatures with nitrates would facilitate the use of metallic masking films if the rate of diffusion can be made reasonably fast at lower temperatures with special glasses.

3. Investigation of the mixing region's design on the output coupling uniformity. Such analysis could improve the circuit design and yield shorter devices with better output coupling uniformity and lower circuit related waveguide losses.

4. Investigation of the diffusion mechanics of the electric field assisted ion-exchange in order to reduce the side diffusion effect and yield a more symmetric waveguide cross-section.

5. Further study of the burying process is required. An electric-field-assisted second diffusion involves the movements of the relatively slow and large thallium ion and the more mobile sodium ions. Optimum choices of electric field and current, second diffusion mixture, and diffusion times must be determined. New masks for the second diffusion may optimize the burying process.

7. References

1. R.H. Doremus, in _Ion Exchange-A Series of Advances_, vol. 2, J.A. Marinsky, ed., Chap, 1, Marcel Dekker, New York (1969).

2. J.R. Tessman and A.H. Kahn, Phys., Rev. 92, 890 (1953).

3. W. A. Weyl and E. C. Marboe, _The Constitution of Glass_, vol. II. Part 2, p. 1086, Wiley, New York (1967).

4. A.D. Pearson, W.G. French, and E.G. Rawson, Appl. Phys. Lett., 15, 76 (1969).

5. W.G. French and A. D. Pearson, Ceramic Bull, 49, 974 (1970).

6. G. Chartier, P. Jaussaud, A. DeLiveira, and O. Parriaux, Electron. Lett., 13, 763 (1977).

7. G. Chartier, P. Collier, A. Guez, P. Jaussaud, and Y. Won, Appl. Opt. 19, 1092 (1980).

8. V. Neuman, O. Parriaux, and L. Walpita, Electron. Lett. 15, 704 (1974).

9. T. Giallorenzi, E. West, R. Kirk, R. Ginther, and R. Andrews, Appl., Opt., 13, 1240 (1973).

10. G. Stewart, C. Miller, P. Laybourn, C. Wilkinson, and R. DelaRue, IEEE J. Quantum Electron. QE-13, 192 (1977).

11. G. Stewart, C. Millar, P. Laybourn, IEEE J. Quantum Electron., QE-14, 132 (1978)

12. G. Chartier, P. Jaussaud, A. de Oliveira, and O. Parriaux, Electron. Lett., 14, 132 (1978).

13. M. Imal, N. Haneda, and Y. Ohtsuka, IEEE J. Lightwave Tech., LT-1, 611 (1983).

14. J. Coutaz and P.C. Jaussaud, Appl. Opt. 21, 1063 (1981).

15. R.K. Lagu and R.V. Ramaswamy, IEEE & OSA 7th Topical Meeting on Integrated and Guided Wave Optics, paper PD8-1, Kissimmee, FL (1984).

16. W.A. Weyl, _Coloured Glasses_, The Scholar Press Limited, Ilkley, Yorkshire, England (1978).

17. P. Ebell, Dingler Polytechnisches Journal, 213, 53 (1874).

18. R. Zsigmondy, Dingler Polytechnisches Journal, 306, 91 (1897).

19. E. Aksenov, N. Esepkina, and A. Lipovskii, Sov. Tech. Phys. Lett. 4, 560 (1978).

20. Y. Won, P. Jaussaud, and G. Chartier, Appl. Phys. Lett., 37, 269 (1980).

21. T. Findakly and B. Chen, Appl. Phys. Lett., $\underline{40}$, 549 (1982).

22. T. Findakly and B. Chen, IEEE & OSA Topical Meeting on Integrated and Guided Wave Optics, Pacific Grove, CA (1982).

23. H. Kita, I. Kitano, T. Uchida, and M. Furukawa, J.Am. Ceramic Soc. 54, 321 (1971).

24. T. Izawa and H. Nakagome, Appl. Phys., Lett. 21, 584 (1972).

25. M. Hatich, D. Chen, and J. Huber, Appl. Phys. Lett. 33, 997 (1978).

26. M. Oikawa, K. Iga, T. Sanada, N. Yamamoto, and K. Nishizawa, Jpn. J. Appl. Phys. 20, L296 (1981).

27. M. Oikawa, H. Wada, and T. Sanada, Electron. Lett. 17, Y52 (1981).

28. E. Okuda, H. Wada, and T. Yamasaki, IEEE & OSA Integrated and Guided Wave Optics Conference, Kissimmee, FL (1984).

29. T. Findakly and E. Garmire, Appl. Phys. Lett. 37, 855 (1980).

30. G. Chartier, P. Jaussaud, A.D. de Oliverira, and O. Parrizux, Electron. Lett. 14, 132 (1978).

31. C.W. Pitt, A.A. Stride, and R.J. Trigle, Electron. Lett. 16, 701 (1980).

32. J. Viljanen and M. Leppihalme, Appl. Phys. 24, 61 (1981).

33. K. Kaede and R.Ishikawa, EUREL 9th European Conference on Opt. Commun., Geneva, Switzerland (1983).

34. See for example: S.M. Sze, Physics of Semiconductor Devices, Wiley, New York (1969).

35. J. Pask and C.W. Parmelee, J. Am. Ceramic Soc. 26, 267 (1943).

36. K. Kobayashi, Appl. Phys. Lett. 31, 374 (1977).

37. F. Heltterrich and M.S. Plesset, J. Chem. Phys. 28, 418 (1958).

38. C.D. Wilkinson and R.Walker, Electron. Lett. 14, 599 (1978).

39. H.J. Lilienhof, E. Voges, D. Ritter, and B. Pantschew, IEEE J. Quantum. Electron. QE-18, 1877 (1982).

40. R.G. Walker, C.D. Wilkinson, and J.A.H. Wilkinson, Appl. Opt. 22, 1923 (1983).

MISSION
of
Rome Air Development Center

RADC plans and executes research, development, test and selected acquisition programs in support of Command, Control, Communications and Intelligence (C^3I) activities. Technical and engineering support within areas of competence is provided to ESD Program Offices (POs) and other ESD elements to perform effective acquisition of C^3I systems. The areas of technical competence include communications, command and control, battle management, information processing, surveillance sensors, intelligence data collection and handling, solid state sciences, electromagnetics, and propagation, and electronic, maintainability, and compatibility.

END

7-87

DTIC